Journal Pre-proofs

Rutaecarpine Derivative Cpd-6c Alleviates Acute Kidney Injury by Targeting PDE4B, a Key Enzyme Mediating inflammation in Cisplatin Nephropathy

Xue-qi Liu, Juan Jin, Zeng Li, Ling Jiang, Yu-hang Dong, Yu-ting Cai, Ming-fei Wu, Jia-nan Wang, Tao-tao Ma, Jia-gen Wen, Ming-ming Liu, Jun Li, Yong-gui Wu, Xiao-ming Meng

PII: S0006-2952(20)30368-3
DOI: https://doi.org/10.1016/j.bcp.2020.114132
Reference: BCP 114132

To appear in: *Biochemical Pharmacology*

Received Date: 5 May 2020
Revised Date: 27 June 2020
Accepted Date: 30 June 2020

Please cite this article as: X-q. Liu, J. Jin, Z. Li, L. Jiang, Y-h. Dong, Y-t. Cai, M-f. Wu, J-n. Wang, T-t. Ma, J-g. Wen, M-m. Liu, J. Li, Y-g. Wu, X-m. Meng, Rutaecarpine Derivative Cpd-6c Alleviates Acute Kidney Injury by Targeting PDE4B, a Key Enzyme Mediating inflammation in Cisplatin Nephropathy, *Biochemical Pharmacology* (2020), doi: https://doi.org/10.1016/j.bcp.2020.114132

Original article

Rutaecarpine Derivative Cpd-6c Alleviates Acute Kidney Injury by Targeting PDE4B, a Key Enzyme Mediating inflammation in Cisplatin Nephropathy

Xue-qi Liu[1,2,#], Juan Jin[3,#], Zeng Li[2,#], Ling Jiang[1,2], Yu-hang Dong[2], Yu-ting Cai[1,2], Ming-fei Wu[2], Jia-nan Wang[2], Tao-tao Ma[2], Jia-gen Wen[2], Ming-ming Liu[2]， Jun Li[2], Yong-gui Wu[1,4*], Xiao-ming Meng[2,*]

1. Department of Nephropathy, the First Affiliated Hospital of Anhui Medical University, Hefei, China

2.The Key Laboratory of Major Autoimmune Diseases, Anhui Institute of Innovative Drugs, School of Pharmacy, Anhui Medical University; The key laboratory of Anti-inflammatory and Immune Medicines, Ministry of Education, Hefei 230032, China.

3. School of Basic Medical Sciences, Anhui Medical University, Anhui, China

4. The Center for Scientific Research of Anhui Medical University, Hefei, China

[#]These authors contribute equally.

*** Corresponding author:**

Professor Xiao-ming Meng, E-mail address: mengxiaoming@ahmu.edu.cn

Professor Yong-gui Wu, wuyonggui@medmail.com.cn

Short title: Rutaecarpine derivative alleviates AKI

Abstract

Acute kidney injury (AKI), characterized by a rapid decline in renal function, is triggered by an acute inflammatory response that leads to kidney damage. An effective treatment for AKI is lacking. Using *in vitro* and *in vivo* AKI models, our laboratory has identified a series of anti-inflammatory molecules and their derivatives. In the current study, we identified the protective role of rutaecarpine (Ru) on renal tubules. We obtained a series of 3-aromatic sulphonamide-substituted Ru derivatives exhibiting enhanced renoprotective and anti-inflammatory function. We identified Compound-6c(Cpd-6c) as having the best activity and examined its protective effect against cisplatin nephropathy both *in vivo* and *in vitro* in cisplatin-stimulated tubular epithelial cells (TECs). Our results showed that Cpd-6c restored renal function more effectively than Ru, as evidenced by reduced blood urea nitrogen and serum creatinine levels in mice. Cpd-6c alleviated tubular injury, as shown by PAS staining and molecular analysis of kidney injury molecule-1 (KIM-1), with both prevention and treatment protocols in cisplatin-treated mice. Moreover, Cpd-6c decreased kidney inflammation, oxidative stress and programmed cell death. These results have also been confirmed in cisplatin-treated TECs. Using web-prediction algorithms, molecular docking, and cellular thermal shift assay (CETSA), we identified phosphodiesterase 4B (PDE4B) as a Cpd-6c target. In addition, we firstly found that PDE4B was up-regulated significantly in the serum of AKI patients. After identifying the function of PDE4B in cisplatin-treated tubular epithelial cells by siRNA transfection or PDE4 inhibitor rolipram, we showed that Cpd-6c treatment did not protect against cisplatin-induced injury in PDE4B knockdown TECs, thus indicating that Cpd-6c exerts its renoprotective and anti-oxidative effects via the PDE4B-dependent pathway. Collectively, Cpd-6c might serve as a potential therapeutic agent for AKI and PDE4B may be highly involved in the initiation and progression of AKI.

Key words: Acute kidney injury; Oxidative stress; Inflammation; Rutaecarpine; Phosphodiesterase enzymes.

Abbreviations

AKI: Acute kidney injury; **Cis**: Cisplatin; **Ru**: Rutaecarpine; **Cpd-6c:**Compound-6c; **TECs**: tubular epithelial cells; **KIM-1**: kidney injury molecule-1; **HK2**: Human tubular epithelial; **CETSA**: cellular thermal shift assay; **PDE4B**: phosphodiesterase 4B; **GFR**: glomerular filtration rate; **RIPK1**: receptor-interacting protein1; **RIPK3**: receptor-interacting protein3; **MLKL**: mixed lineage kinase domain-like protein; **ROS**: reactive oxygen species; **NOX:** NADPH oxidases; **BUN**: blood urea nitrogen

Chemical compounds

Chemical compounds enlisted in this article: Rutaecarpine (PubChem CID: 65752).

1. Introduction

Acute kidney injury (AKI) is a clinical syndrome caused by multiple factors, including ischemic-reperfusion injury, drug toxicity (such as cisplatin), and sepsis (1-4). A common symptom is decreased glomerular filtration rate (GFR) accompanied by retention of nitrogen metabolites such as creatinine, urea nitrogen, and water, electrolyte imbalance, and acid-base balance disorders (5-7). Although inflammation ,oxidative stress and programmed cell death were shown to play critical roles in AKI, it is vital to identify the potential underlying mechanisms and to develop effective treatment options (8, 9).

We screened several anti-inflammatory molecules and their derivatives using cisplatin-treated tubular epithelial cells (TECs). Our previous studies showed the protective role of protocatechuic aldehyde in attenuating cisplatin-induced AKI by inhibiting NOX-mediated oxidative stress and p65 NF-κB-driven renal inflammation(10).Wogonin protects against nephrotoxic AKI by targeting receptor-interacting protein1 (RIPK1)-mediated necroptosis and 7-Hydroxycoumarin attenuates AKI by limiting necroptosis while promoting Sox9-mediated tubular epithelial cell proliferation

(11, 12). The major finding of this study is that Ru and its derivatives show a cytoprotective effect. Rutaecarpine officinalis sub alkaloid, the principal component of *Evodia officinalis* (13-15), is a natural alkaloid. There are reports that it has a wide range of pharmacological activities, including inhibition of oxygen-free radical release, anti-inflammation,, and immunomodulation (16-20). Whether Ru and its derivatives exert protective effects on nephrotoxic AKI, and whether its derivatives exhibit a higher protective effect require critical evaluation.

In this study, we identified 3-aromatic sulphonamide-substituted Ru derivative, Cpd-6c, as the most potent compound for reducing cisplatin-induced renal damage, inflammatory response and oxidative stress. Necroptosis is a form of programmed cell death and dependent on receptor interacting protein kinase (RIPK)1 and is regulated by RIPK3 and its substrate mixed lineage kinase domain-like protein (MLKL) that plays an important role in AKI(21). Results presented here show that Cpd-6c suppressed cisplatin-induced cell necroptosis. Now the evidence is also clear that oxidative stress is a major factor in AKI and superoxide derived from NADPH oxidase is the core of oxidative stress(22-24). NOX1, NOX2 and NOX4 as the major NADPH isoforms in kidney was significantly down-regulated by Cpd-6c. Furthermore, we showed that the Cpd-6c exert its renoprotective mechanism by interacting with PDE4B, a newly identified pro-inflammatory enzyme involved in cisplatin nephropathy. For the first time, we found that PDE4B was up-regulated significantly in the serum of AKI patients and interference with PDE4B expression regulated cellular oxidative stress. To verify potential interactions between Cpd-6c and PDE4B protein, we used molecular docking studies and cellular thermal shift assays (CETSA). Our findings identified a novel small molecule that prevented kidney damage in cisplatin-induced AKI. Furthermore, PDE4B could be served as a potential target for treating nephrotoxic AKI.

2. Materials and methods

2.1 Reagent and materials

Ru was purchased from Aladdin Biotechnology Co., Ltd. (Shanghai, China, CAS NO: 84-26-4, Item-NO: R107338, Lot-NO: A1904074). The Purity of Ru was more than 98% and proton NMR spectrum conforms to structure. Ru's derivatives were synthesised at the School of Pharmacy,

Anhui Medical University. Early stage of our laboratory has synthesized a series of derivatives by modifying the structure of Ru to increase its selectivity and reduce its side effects. The synthesis method is detailed in our previous report(19). The structures of compounds are shown in **Figure 1A**. And the minimum characterization of Cpd-6c is shown in **Figure 1B**. Specific antibodies against TNF-α, P-P65, P65, RIPK1, RIPK3, and β-actin were obtained from Santa Cruz Biotechnology (CA, U.S.A). The antibodies against kidney injury molecular-1 (KIM-1), rabbit anti-P-MLKL, anti-cleaved caspase-3, PDE4B, and 3,5-cyclic adenosine monophosphate (cAMP) were purchased from Cell Signalling Technology (Danvers, MA, U.S.A.). Anti-PDE4D and anti-PDE10A were purchased from Abcam (Cambridge, UK). Anti-Nox1, anti-Nox2, and anti-Nox4 were purchased from Bioss Biotechnology (Bioss, Beijing, China). Rolipram was obtained from Sigma-Aldrich (Shanghai, China). Protein assay kit was purchased from Beyotime Institute of Biotechnology (Jiangsu, China). Lipofectamine 2000 was purchased from SciencBio Technology (Invitrogen, Carlsbad, CA, USA). Periodic acid-Schiff (PAS), blood urea nitrogen (BUN), and creatinine kits were purchased from Nanjing Jiancheng Bioengineering Institute (Jiangsu, China). The dihydroethidium (DHE) and reactive oxygen species assay (DCF Assay) kits were obtained from Beyotime Institute of Biotechnology (Jiangsu, China).

2.2 Establishment of cisplatin-induced AKI mouse model

Male C57BL/6J mice (approximately 20– 22 g) were provided by the Experimental Animal Centre, Anhui Medical University. All animal procedures were approved by the Animal Experimentation Ethics Committee of the Anhui Medical University, Anhui, China and conducted by GUIDE LABORATORY ANIMALS FOR THE CARE AND USE OF Eighth Edition. A total of 56 mice were divided into seven groups (n=6-8). The 8-week-old mice were injected with 20 mg/kg of cisplatin, while the control group was injected with the same amount of saline. In protocol I, Cpd-6c concentrations of 25, 50, and 100 mg/kg were administered intraperitoneally 12 h before cisplatin treatment and injected daily. In protocol II, Cpd-6c was intraperitoneally injected 24 h after cisplatin injection and then injected once daily for three days. Animals were humanely killed by exsanguination under inhaled 5% isoflurane anaesthesia three days after the injection of cisplatin. We collected the tissue and blood samples for the detection of blood urea

nitrogen (BUN) and creatinine, PAS staining and molecular analysis.

2.3 ELISA

Clinical experiments were approved by the ethics committee of The First Affiliated Hospital of Anhui Medical University. According to the KDIGO criteria, AKI is diagnosed if SCr increases by 0.3 mg/dl (or≥ 26.5 mM) in≤ 48 h or increases to≥ 1.5-fold from baseline within the prior 7 days and/or by a decrease in urine output of < 0.5 ml/kg/h for 6-12 h. After obtaining patient and ethics committee consent, serum from healthy volunteers and patients with AKI were collected and processed within 6h of collection (n=6). The level of PDE4B was detected using ELISA Kit (Jianglai Biotechnology Co., LTD, Shanghai, China) according to the manufacturer's instructions. Purified monoclonal antibody against PDE4B in an ELISA kit. The group consists of blank holes, standard holes and sample holes. Serum samples were added to the coated microwells in sequence (no serum samples and enzyme-labeled reagents were added to the blank control wells, standard holes were added with different concentrations of standard substance), and then combined with horseradish peroxidase(HRP)-labeled detection antibodies to form antibody-antigen-enzyme-labeled antibody complexes. The substance tetramethylbenzidine is converted into blue under the catalysis of HRP enzyme, and finally into yellow under the action of acid. The color depth is positively correlated with the content of human PDE4B in the sample. The absorbance was determined using a microplate reader (Multiskan MK3, Thermo, USA) at a wavelength of 450 nm for optical density (OD) measurements.

2.4 Cell culture

Human kidney tubular epithelial cells (HK2) were provided by Professor Huiyao Lan of the Chinese University of Hong Kong. Cell lines validation was carried out by Biowing Applied Biotechnology Co. Ltd (Shanghai, China) by means of DNA Profile STR (Short Tandem Repeat). Cells were cultured in HyCloneTM DMEM/F12 medium with 5% FBS at 37°C in humidified 5% CO_2, and cells between passages 6-15 were used in experiments. Starved cells were pre-treated with Ru and its derivatives, then cells were treated with cisplatin (20μM) and incubated for 24 h.

Cells were harvested after 24 h for further analysis.

2.5 MTT assay

We used the MTT assay to detect cell viability. Human HK2 cells were grown in 96-well plates and treated with varying concentrations of Ru and its derivatives for 12 h, or cisplatin for 24 h before the addition of 5 mg/mL of MTT solution for 4 h. The absorbance was determined using a microplate reader (Multiskan MK3, Thermo, USA) at a wavelength of 492 nm for optical density (OD) measurements. The concentration for 50% of maximal effect (EC50) values were calculated by GraphPad Prism 5.0 software (GraphPad Software, Inc, San Diego, CA).

2.6 PDE4B knockdown in HK2 cells by transfecting siRNA

PDE4B siRNA (GenePharma, Shanghai, China) was transfected into human kidney TECs by adding Lipofectamine TM 2000 reagent (Invitrogen) following the manufacturer's protocol. We used the negative scrambled siRNA (GenePharma, Shanghai, China) as a control. The diluted siRNA and Lipofectamine 2000 were combined and incubated for 15 min at 37℃ in the dark, and the mixture added to cells. After incubation for 6 h, the cells were grown in 5% FBS-containing DMEM-F12. Cells with PDE4B siRNA were cultured at 37°C in an atmosphere containing 5% CO_2.

2.7 RNA extraction and real-time PCR

Total RNA was extracted from freshly isolated kidney tissues or cultured HK2 cells by RNA-iso reagent (TakaRa). RNA concentration was detected using the NanoDrop 2000 spectrophotometer (Thermo Scientific, USA), and cDNA prepared by reverse-transcription with RealMasterMix (TOYOBO, Japan). SYBR-Green I Real-time quantitative PCR with a CFX96 real-time RT-PCR detection system (Bio-Rad, U.S.A.) was used to determine the levels of KIM-1, IL-6, IL-8, TNF-α, PDE4B, and β-actin. The sequences of the primers are listed in **Table 1.**

PCR amplification was carried out over 40 cycles using the following conditions: denaturation at 95℃ for 20 seconds, annealing at 58℃ for 20 seconds, and elongation at 72℃ for 20 seconds. The mRNA expression values were normalized to that of β-actin.

2.8 Western blotting analysis

Proteins from renal tissues or cells were isolated with cold RIPA-Buffer (Beyotime, Jiangsu, China), and their concentrations quantified by BCA protein kit (Beyotime, Jiangsu, China). Then, they were separated on different concentrations of SDS-PAGE gels and transferred to nitrocellulose membranes. The membrane was incubated overnight at 4℃ with primary antibodies against KIM-1, P-P65, P65, PDE4B, RIPK1, RIPK3, P-MLKL, cleaved caspase-3, and β-actin, washed, and incubated for 1.5 h at 37℃ with IRDye 800-conjugated secondary antibody (1:10,000; Rockland Immunochemicals, Gilbertsville, PA, USA). The developed band intensities were detected by LiCor/Odyssey infrared image system (LI-COR Biosciences, Lincoln, NE, USA), and images quantified using the Image J software (NIH, Bethesda, MD, USA).

2.9 Immunofluorescence assay

For PDE4B and cAMP immunofluorescent staining, the HK2 cell monolayers were grown on slides and fixed with 4% acetone for 10 minutes. After washing with PBS three times, they were blocked with 10% bovine serum albumin at room temperature and incubated at 4˚C overnight with primary antibodies, rabbit anti-PDE4B and anti-cAMP. After washing three times, the goat anti-rabbit IgG-rhodamine (Bioss, Beijing, China) antibody was added and incubated for 1 h in the dark at room temperature. The nuclei were stained by incubation with DAPI for 5 min. After three washes with PBS, slides were imaged with an inverted fluorescence microscope (Zeiss Spot; Carl Zeiss MicroImaging GmbH, Gottingen, Germany).

2.10 Molecular docking

For identifying the potential interactions between the tested compound and PDE4B protein, molecular docking studies were performed using the Discovery Studio 2017 R2 (BIOVIA Software, Inc., San Diego, CA, United States). The X-ray crystal structure of PDE4B (PDB ID: 3O0J) complexed with 3OJ inhibitor was obtained from the RCSB Protein Data Bank (New York, NY, USA). Protein and ligand were prepared for docking, and the CDOCKER protocol was used to identify the potential inhibitor binding site on PDE4B. The binding pocket was defined using the centre of the native ligand 3OJ, and docking parameters were set to default.

2.11 Cellular thermal shift assay (CETSA)

Cells were treated with or without Cpd-6c after which, RIPA lysis buffer was added. Total protein was quantified using a protein assay kit (Beyotime, Jiangsu, China), and samples adjusted to similar final concentrations. Equal aliquots were placed in different PCR tubes, and samples were denatured for 8 min at varying temperatures in the PCR instrument (Eppendorf, Germany). The samples were freeze-thawed three times using liquid nitrogen, and centrifuged; the supernatants were analysed using western blot.

2.12 DCF Assay

The DCF is an oxidation product of 2,7-dichlorodihydro-fluorescein diacetate, an indicator of cellular oxidation. The cells produce ROS after cisplatin treatment, measured as an increase in fluorescence from 2,7-dichlorodihydrofluorescein, and imaged at 488 nm using a fluorescence microscope (Leica, Bensheim, Germany). Cells were incubated with DCF (10 mL/L) for 20 min at room temperature in DMEM/F12 medium without FBS.

2.13 DHE Staining

The cellular ROS levels from the oxidation of DNA were estimated by measuring the red-fluorescent DHE product. Cells were incubated with 5 mM fresh DHE solution (Beyotime, Jiangsu, China) for 30 min at 37°C. After washing with serum-free medium, fluorescence was measured with a fluorescence microscope.

247

248 **2.14 Flow cytometry**

249 For evaluating apoptotic programmed cell death, both attached and floating cell population were
250 incubated with 10 µL of annexin V-FITC and 5 µL of PI in the dark, and analysed on a BD
251 FACSVerse flow cytometer machine (BD FACSVerse, BD Biosciences, Franklin Lakes, NJ,
252 USA). The data were analysed by the FlowJo 7.6 software.

253

254 **2.15 Histology, immunohistochemistry, and morphological assessment**

255 Kidneys were collected and fixed in 4% paraformaldehyde overnight. Fixed kidney samples were
256 embedded in paraffin and sliced into 4µm sections. The extent of the renal tubular interstitial
257 injury was evaluated by PAS staining of paraffin sections following the manufacturer's
258 instructions, and examined by microscope (Leica, Bensheim, Germany) at 200× magnification.
259 The PAS-stained renal sections (n = 6–8) were evaluated for the proximal cortical renal damage
260 score defined by the degree of tubular necrosis, cast formation, and tubular dilation, as shown
261 here, 0 = normal; 1 = 10%; 2 = 10-25%; 3 = 26-50%; 4 = 51-75%; 5 = 75-95%; 6 = greater than
262 96%. For immunohistochemistry, the kidney sections were treated with 0.01 M sodium citrate
263 buffer (pH = 6.0), and antigen retrieval was conducted using a microwave-based technique by
264 heating sections at 95℃ for 20 min, followed by 10 min in 3% H_2O_2 to block endogenous
265 peroxidase activity. Next, the sections were incubated at 4℃ with rabbit anti-TNF-α, anti-PDE4B,
266 and anti-KIM-1 antibodies for 24 h, washed and incubated for 30 min at 37℃ with secondary
267 antibodies. After DAPI staining, the slides were visualized under a microscope (Leica, Bensheim,
268 Germany).

269

270 **2.16 Statistical analyses**

271 All data were expressed as the mean ± SEM, and the one-way analysis of variance (ANOVA) was
272 used for data analysis, followed by Tukey's posthoc tests using the GraphPad Prism 5 software.

273

3. Results

3.1 Rutaecarpine (Ru) and its derivatives suppress cisplatin-induced death in renal tubular epithelial cells

The molecular structures of compounds are shown in **Figure 1A**. We used the MTT assay to assess the cytotoxicity of Ru and its derivatives and to determine the optimal concentration for use in our experiments (**Figure 2A**). The results of MTT assay showed that Ru treatment affected cell viability at concentrations exceeding 2 μM. However, the cell viability was unaffected at Ru concentrations of 0.25, 0.5, and 1 μM in cisplatin-treated HK2 cells. The results showed that only Cpd-6c and Cpd-6b could restore cell viability. The concentration of the Cpd-6c was less than 4.8 μM while that of Cpd-6b was less than 2.4μM, and these compounds showed a minimal effect on HK2 cell viability. Meanwhile, EC50 values was 4.4μM for Cpd-6c and 9.9μM for Cpd-6b. When they at concentrations of 0.6, 1.2, 2.4μM, and 0.3, 0.6, 1.2μM, respectively, restored the viability of cisplatin-treated HK2 cells. We further assessed the effect of Cpd-6c and Cpd-6b by examining the changes in KIM-1 protein levels. The results of the western blot showed that cisplatin upregulates KIM-1, and although both Cpd-6c and Cpd-6b reduce KIM-1 expression, Cpd-6c was more effective than Cpd-6b (**Figure 3A**). We, therefore, chose Cpd-6c for further examination. Results showed that Cpd-6c reduces KIM-1 levels by real-time PCR and immunofluorescence (**Figure 3B and 3C**). In addition, we used flow cytometric analysis of PI/Annexin V stained cells to test and validate the role of Cpd-6c in protection against HK2 cell death. Flow cytometry data showed that Cpd-6c alleviates cisplatin-induced programmed cell death. Cisplatin (20μM) induced programmed cell death in TECs. However, the ratios of both annexin V-FITC+/PI+ (late apoptotic or necrotic) and annexin V-FITC+/PI- (early apoptotic) cells decreased in response to Cpd-6c treatment (**Figure 3D**). Moreover, the level of cleaved caspase-3 was also significantly downregulated (**Figure 3E**). In addition, Cpd-6c dose-dependently caused a significant decrease in signalling molecules that mediate necroptosis, RIPK1 and RIPK3 levels, and phosphorylation of the downstream mixed lineage kinase domain-like protein (MLML) in HK2 cells (**Figure 3E**).

3.2 Cpd-6c reduces the cisplatin-induced inflammation response

We examined the p65 NF-κB phosphorylation level (**Figure 4A**) to assess whether Cpd-6c reduces inflammation. Moreover, real-time PCR analysis confirmed the protective effect of Cpd-6c on the inflammatory response, as evidenced by decreased levels of inflammatory cytokines such as IL-1β, IL-8, and TNF-α (**Figure 4B**).

3.3 Cpd-6c suppresses cisplatin-induced cell injury by attenuating NOX-mediated oxidative stress

Several major NOX family members, including NOX1, NOX2, and NOX4, were identified, and western blot analysis results showed that Cpd-6c treatment caused a decrease in cisplatin-induced upregulated NOX levels (**Figure 4C**). The results showed that Cpd-6c significantly reduced reactive oxygen species (ROS) levels in cisplatin-treated HK2 cells. DCF fluorescence in HK2 cells was measured for evaluating the effect of Cpd-6c on oxidative stress (**Figure 4D**). Consistently, the results of DHE staining showed that superoxide levels and NOX enzyme products were inhibited by Cpd-6c (**Figure 4E**).

3.4 Cpd-6c Target prediction

Cpd-6c target prediction was performed using the Discovery Studio 2017 (DS 2017) software. As shown in **Figure 5A,** the binding strength of Cpd-6c and the potential target is represented by the colour red to blue. The fit values indicate the scores of the hypothetical targets, and the top ten disease-related targets are shown in **Table 2**. Among these targets, the fit value of PDE4B, a critical inflammation-related target in renal injury, was high with a fit value of 0.9868 and appeared at a higher frequency, as shown in the mapping.

3.5 Cpd-6c binds directly to PDE4B as shown by CETSA and molecular docking

Interestingly, we detected PDE4B release using serum from healthy volunteers and patients with AKI, result showed that the serum PDE4B content of AKI patients increased significantly, this

result indicates that PDE4B may be highly involved in the pathophysiological process of AKI. (**Figure 5B**). Then, we verified the interaction between Cpd-6c with PDE4B, PDE4D and PDE10A proteins by performing CETSA tests, enabling us to evaluate target engagement *in vivo*. Results show varying levels of soluble PDE4B at denaturation temperatures ranging from 60–70°C with and without Cpd-6c treatment. Cells treated with Cpd-6c had significantly higher thermally stable PDE4B, indicating that Cpd-6c binds directly to the PDE4B protein (**Figure 5C**).

The mechanism by which Cpd-6c suppresses the release of inflammatory cytokines was elucidated by molecular docking analysis of the binding mode between Cpd-6c and PDE4B (PDB ID: 3O0J) (**Figure 5D)**. The most stable binding pose in the active site of PDE4B was illustrated and analysed through 2D and 3D diagrams. The docking results for the interaction of the tested compound with PDE4B showed the highest interaction energy score of 53.6216 kcal/mol using CDOCKER_INTERACTION_ENERGY analysis. As shown in Figure 5D, the tested compound bound to the active site of PDE4B by two hydrogen bonds interacting with ASP346 and HIS234 and two carbon-hydrogen bonds interacting with ASN395 and GLN443. Furthermore, other binding interactions, such as pi-sulphur, pi-pi stacked, pi-pi t-shaped, and pi-alkyl, contribute to the binding affinity. These results suggest that the anti-inflammatory activity of the tested compound might be due to its binding to the PDE4B protein

3.6 Cpd-6c attenuates PDE4B signalling in cisplatin-treated HK2 cells

The bioinformatic prediction website suggests that Cpd-6c may bind to the PDE4B target. Immunofluorescence results showed significantly downregulated PDE4B levels in response to Cpd-6c treatment (**Figure 5E**). Additionally, cAMP levels, the substrate for PDE4B enzyme, increased significantly, as shown by immunofluorescence (**Figure 5F**).

3.7 Cpd-6c suppresses *in vitro* cisplatin-induced cell injury by blocking a PDE4B instead of PDE10A and PDE4D-dependent mechanism

The PDE4B, PDE10A and PDE4D in HK2 cells was knocked down by siRNA transfection. The

355 results showed markedly decreased PDE4B, PDE10A and PDE4D mRNA and protein levels in
356 HK2 cells (**Figure 6A-B**). We showed that after PDE4B knockdown, Cpd-6c failed to reduce
357 renal cell injury. When PDE4B was inhibited, Cpd-6c was unable to suppress KIM-1 (**Figure**
358 **6C-D**). Results showed that although silence of PDE4D or PDE10A slightly attenuated renal
359 injury, when PDE4D and PDE10A was loss, Cpd-6c was still able to suppress KIM-1 level
360 (**Figure 6E-F**). This indicated that Cpd-6c may suppress cell injury in PDE4D or
361 PDE10A-independent mechanism.

362

363 **3.8 Cpd-6c suppresses *in vitro* cisplatin-induced inflammatory response and oxidative stress**
364 **by blocking a PDE4B -dependent mechanism**

365 When PDE4B was inhibited, Cpd-6c was unable to suppress cleaved caspase-3 levels (**Figure**
366 **7A**). After the knockdown of PDE4B, Cpd-6c failed to reduce the renal inflammatory response
367 further. Results showed that PDE4B inhibition significantly decreased cisplatin-induced P65
368 protein phosphorylation, and NF-κB-mediated inflammatory response, which could not be
369 downregulated further by Cpd-6c in the absence of PDE4B (**Figure 7B**). Moreover, real-time PCR
370 showed that Cpd-6c did not further decrease the levels of inflammatory cytokines such as TNF-α,
371 IL-1β, and IL-8 in the absence of PDE4B (**Figure 7C**). Importantly, we found that Cpd-6c was
372 unable to suppresses NOX-mediated oxidative stress after PDE4B knockdown, thus indicating that
373 Cpd-6c exerts its activity primarily through PDE4B (**Figure 7D**).

374

375 **3.9 Targeting PDE4B with Cpd-6c leads to enhanced protection from cisplatin-induced cell**
376 **injury compared to that observed using a classic PDE4 inhibitor rolipram**

377 Rolipram is a well-known PDE4 inhibitor that reduces inflammation in a variety of organs,
378 including the kidney. In this study, we evaluated the protective effect of rolipram on HK2 cell
379 viability, and results identified an optimal rolipram concentration of 0.25μM **(Figures 8A and**
380 **8B).** The results of western blot and real-time PCR revealed a stronger inhibitory effect on KIM-1
381 protein and mRNA levels via selective PDE4B inhibition by Cpd-6c compared to that observed
382 upon the broad inhibition of PDE4 by rolipram **(Figures 8C and 8D).** Furthermore, pre-treatment

with Cpd-6c had a better suppressive effect on cisplatin-induced apoptosis, NOX-mediated oxidative stress and inflammation, compared to that of rolipram **(Figures 8E-H).**

3.10 Cpd-6c inhibits cisplatin-induced acute kidney injury in mice

We further evaluated the renoprotective effect of Cpd-6c on cisplatin-induced AKI in mice. Cpd-6c improved renal function, as evidenced by serum creatinine and BUN values (**Figures 9A and 9B**). The results of PAS staining showed that Cpd-6c at concentrations of 25, 50, and 100 mg/kg.day^{-1}, reduced tubular dilation, tubular necrosis, and cast formation. Moreover, the results of PAS staining showed that Cpd-6c reduced vacuolar degeneration in renal tubular epithelial cells, renal interstitial oedema, and inflammatory cell infiltration (**Figure 9C**). In addition, western blot results showed marked upregulation of KIM-1—a key renal tubule injury factor—by cisplatin that decreased dose-dependently upon Cpd-6c treatment, consistent with results from real-time PCR and IHC (**Figures 9D-F**).

3.11 Cpd-6c ameliorates cisplatin-induced up-regulation of PDE4B and inhibits programmed cell death

We tested whether Cpd-6c affects PDE4B in cisplatin-treated mice by measuring PDE4B levels by western blot and immunohistochemistry. Results showed that the PDE4B levels increased in response to cisplatin, but decreased upon treatment with Cpd-6c (**Figures 10A and 10B**). Furthermore, Cpd-6c suppressed RIPK1-dependent necroptosis signalling, including activation of the RIPK1/RIPK3/MLKL axis, and apoptosis-correlated cleavage of caspase-3. These findings illustrated the protective effects of Cpd-6c on cisplatin-induced renal programmed cell death *in vivo* (**Figure 10C**).

3.12 Cpd-6c protects against cisplatin-induced nephropathy by ameliorates inflammatory response and NOX-mediated oxidative stress

We tested the anti-inflammatory effect of Cpd-6c in cisplatin-treated mice and showed that Cpd-6c reduced the mRNA levels of TNF-α, IL-1β, and IL-6 significantly (**Figure 11A**). Results from western blot analysis showed that Cpd-6c suppressed P65 phosphorylation in cisplatin-treated kidneys (**Figure 11B**). Immunohistochemistry data also showed that Cpd-6c decreased the TNF-α level (**Figure 11C**). Moreover, Results from western blot analysis showed that Cpd-6c inhibited NOX-mediated oxidative stress. (**Figure 11D**).

3.13 Cpd-6c attenuated cisplatin-induced kidney injury in established AKI mouse model

To determine the therapeutic potential of Cpd-6c in an established AKI mouse model, we treated mice with Cpd-6c one day after cisplatin injection. Results show that Cpd-6c improved renal function supported by serum creatinine and BUN assays (**Figure 12A and 12B**). PAS staining also showed Cpd-6c attenuated kidney damage (**Figure 12C**). This was further supported by results from western blot of KIM-1 (**Figure 12D**).

4. Discussion

Recently, AKI has been found to be associated with high incidence and mortality rates, especially among inpatients; however, the best treatment strategy is yet to be discovered (4, 23). In this study, we showed that Cpd-6c was more effective in alleviating nephrotoxic AKI by suppressing renal inflammatory response and renal oxidative stress by interacting with PDE4B, a newly identified pro-inflammatory enzyme in cisplatin-induced nephropathy.

Ru is a quinazoline carboline alkaloid isolated as one of the active ingredients of the medicinal plant *Evodia rutaecarpa* (25). Ru has been reported to reduce inflammation, and to inhibit the release of oxygen free radicals and adhesion molecules while regulating immunity (26) in several diseases. Ru targets VEGFR2 to inhibit angiogenesis and protects HPASMCs against hypoxia partly via the HIF-1α-dependent signalling pathway (13, 20). In addition, Ru has a significant effect on the proliferation and apoptosis of human tumour cells (27-29). However, the role of Ru

436 in nephrotoxic renal injury and enhancement of its renoprotective effect by modifying its chemical
437 configuration requires further research. In this study, the relationship between its
438 structure-activity, by modifying its structure to improve its selectivity and reduce its side effects
439 was examined by attaching an aromatic sulphonamide group at the 3-position of Ru. Among them,
440 Cpd-6c, containing $–OCH_3$ at the C2 and C3 positions of the benzene ring, showed a significantly
441 increased renoprotective effect, antioxidant and anti-inflammatory activity compared to that of the
442 parent drug and other derivatives with thiophene rings.

443

444 In the present study, we showed the *in vivo* and *in vitro* anti-inflammatory activity of Cpd-6c on
445 cisplatin-induced damage. Inflammation is a complex biological response necessary for
446 eliminating microbial pathogens, and to repair damaged tissue. AKI is a systemic
447 inflammation-related condition. Therefore, understanding the underlying cellular and molecular
448 mechanisms of inflammation enables the identification of effective treatments to prevent or treat
449 AKI. Recent research identified multiple AKI-associated inflammatory response signals, including
450 the molecular signals released by dying cells, the role of pattern recognition receptors, the diverse
451 subtypes of resident and recruited immune cells, and the phased transition from destructive to
452 reparative inflammation (30). Cpd-6c treatment of mice with cisplatin-induced AKI showed
453 significantly suppressed inflammation,

454

455 The current study results also showed that Cpd-6c inhibits oxidative stress by reducing ROS
456 production in TECs and in renal tissues treated with cisplatin. There is substantial evidence that
457 oxidative damage to renal tissue and tubular cells is associated with AKI. During the onset of
458 AKI, ROS levels increase early and involve in the pathological processes of different types of
459 AKI(31, 32). Increased oxidative damage and decreased tissue antioxidant status will occur after
460 renal ischemia or nephrotoxicity(33).Oxidative stress refers to the serious imbalance between free
461 radical production and antioxidant defence when the body is subjected to various harmful stimuli,
462 which leads to tissue damage. Existing evidence shows the involvement of oxidative stress in the
463 pathogenesis of cisplatin-induced nephrotoxicity (34). NADPH oxidase—a membrane-bound

protein—and ROS in the kidney are produced through NADPH when it transfers electrons across biological membranes (10, 35). NOXs 1–5, DUOX1, and 2 belong to the NOX family. The NOX2 and NOX4 are expressed highly in the kidney, although NOX4 is the dominant form with critical roles in renal oxidative stress and kidney damage (22, 31, 36, 37). Inflammation is closely related to oxidative stress, and emerging evidence shows that severe inflammatory response triggers tissue injury and causes excessive ROS production (22, 38). Treatment with Cpd-6c reduced inflammation and oxidative stress.

Additionally, we found that Cpd-6c alleviates cisplatin-induced programmed cell death significantly, especially necroptosis and apoptosis. Necroptosis is a type of programmed cell death characterised by an impaired plasma membrane that allows cell contents to escape, leading to inflammation (9, 39, 40). Necroptosis is a receptor-interacting protein kinase (RIPK)1-dependent process and is regulated by RIPK3 and its substrate mixed lineage kinase domain-like protein (MLKL). Compared to apoptosis, necroptosis plays a more critical role in the inflammatory response of renal TECs (41-43). As the cell membrane collapses, several damage-associated molecular patterns (DAMPs), including heat-shock proteins, uric acid, high-mobility group box 1 (HMGB1), and IL-33 are released (11, 34). These DAMPs trigger renal inflammation-related signalling pathways by interacting with specific receptors resulting in renal inflammation and necroinflammation, causing more necroptosis in the injured kidney, thus forming a positive-feedback loop (41, 44). In addition, previous studies have shown that ROS increases cellular oxidative stress, which in turn leads to DNA damage and programmed cell death(31). ROS scavengers can significantly reduce hypoxia/reoxygenation-induced cell necrosis(45). Importantly, we found that Nox-mediated oxidative stress is closely related to programmed cell death(22).

Another important finding of the current study is PDE4B could be used as a novel target for cisplatin-induced renal inflammation and oxidative stress. The phosphodiesterase 4 (PDE4) family comprises four genes, PDE4A, B, C, and D, which encode more than 20 isoforms (46-48). Cyclic

492 nucleotide phosphodiesterase enzymes (PDEs) negatively regulate cyclic adenosine
493 monophosphate (cAMP) levels and covert cAMP into 5'-adenosine monophosphate (AMP)
494 (49-51). cAMP is a key modulator of cellular homeostasis that regulates vascular tension and
495 endothelial permeability, thereby contributing to immune cell activation and inflammation (49,
496 52-54). Following spinal cord injury, PDE4B plays a critical role in the progression of acute and
497 chronic local inflammatory response, as well as that of systemic response aggravated by gut
498 dysbiosis and endotoxemia (55). As cAMP is known to be a critical mediator of many renal
499 functions, including solute transport, regulation of vascular tone, the proliferation of parenchymal
500 cells, and inflammation, some studies have shown the therapeutic potential of a targeted PDE4
501 inhibitor in progressive renal disease (56, 57). Rolipram, a PDE4 inhibitor, restores renal function
502 in patients with sepsis, despite the production of oxidants even with delayed treatment (58). Drug
503 discovery and clinical development studies on PDE4 inhibitors such as rolipram were performed
504 in the 1980s, but were hampered severely due to significant side-effects such as nausea and emesis
505 (52, 56, 59). PDE4B is the primary phosphodiesterase involved in inflammation; However, its
506 selective inhibitor has not yet been developed.

507

508 In the current study, results show that Cpd-6c plays an effective role in renal protection; we
509 further identified its mechanisms of action. The molecular targets of Cpd-6c were predicted using
510 the DS software. Cpd-6c interaction with PDE4B was identified through computer-aided
511 simulation. Target engagement (TE) is a critical factor for evaluating drug potential during its
512 development. The intracellular TE could be measured by cellular thermal shift assay (CETSA) at
513 all stages of drug development (43, 60). To determine whether PDE4B, PDE10A or PDE4D are
514 the potential drug targets, the result of CETSA showed that cells treated with Cpd-6c didn't have
515 significantly higher thermally stable PDE4D and PDE10A, indicating that Cpd-6c didn't bind
516 directly to the PDE4D and PDE10A proteins. On the contrary, the thermal stability of PDE4B
517 protein was significantly improved in Cpd-6c treated cells, indicating that Cpd-6c directly bound
518 to PDE4B protein. The most stable binding pose in the active site of PDE4B was illustrated and
519 analysed through molecular docking. Importantly, we first found that PDE4B was up-regulated
520 significantly in the serum of AKI patients which indicates that PDE4B may be highly involved in

521 the initiation and progression of AKI.

522

523 Currently, we confirmed cisplatin-induced upregulation of PDE4B protein level *in vitro*
524 cisplatin-treated HK2 cells as well as *in vivo* cisplatin-induced nephropathy were substantially
525 reversed by Cpd-6c treatment. Additionally, we showed that PDE4B, PDE10A and PDE4D
526 knockdown or treatment with rolipram attenuated cisplatin-induced renal inflammation and
527 programmed cell death. At the same time, we also detected whether Cpd-6c functions through
528 PDE4B, PDE10A or PDE4D. *In vitro* results from PDE4B knockdown cells indicated that Cpd-6c
529 showed no further reduction in cisplatin-induced high levels of KIM-1, cleaved caspase-3, and
530 production of inflammatory factors. However, when PDE4D and PDE10A was loss, Cpd-6c was
531 still able to suppress KIM-1 level. We confirmed that Cpd-6c suppresses cisplatin-induced cell
532 injury by blocking a PDE4B instead of PDE10A and PDE4D-dependent mechanism. Importantly,
533 for the first time, we found that silencing PDE4B also reduces oxidative stress in AKI. In our
534 previous study, we found that Protocatechuic Aldehyde blocks cisplatin-induced AKI by
535 suppressing Nox-mediated oxidative stress and RIPK1 inhibitor Cpd-71 attenuates renal
536 dysfunction in cisplatin-treated mice via attenuating necroptosis and oxidative stress(10, 60), and
537 here we discovered Cpd-6c relieves oxidative stress injury through PDE4B-dependent pathway.
538 The above results suggest that Cpd-6c may exert its anti-inflammatory and antioxidant role in
539 cisplatin-induced nephrotoxicity by targeting PDE4B. Additionally, reduced PDE4B protein levels
540 observed in response to Cpd-6c in the cisplatin-treated group may be the result of an indirect
541 effect of decreased inflammation leading to lower PDE4B level in a positive feedback loop, and
542 warrants further investigation. Furthermore, our results showed an enhanced therapeutic effect of
543 Cpd-6c compared to that of the classical PDE4 inhibitor, rolipram, in cisplatin-stimulated tubular
544 epithelial cells. Considering the low cytotoxicity of Cpd-6c, it may serve as a potential therapeutic
545 agent against nephrotoxic AKI.

546

547 Collectively, our study confirms the renoprotective effect of Cpd-6c on cisplatin-induced AKI by
548 targeting PDE4B-dependent inflammation and oxidative stress. Therefore, inhibiting the

549 expression of PDE4B with Cpd-6c could be considered as a potential and novel therapeutic
550 strategy for AKI.

551

552 **Author Contributions**

553 X.Q. Liu, J. Jin, and L. Jiang conducted the experiments and analysed the data. X.Q. Liu and X.M.
554 Meng wrote the manuscript. Z. Li conceived the molecular docking experiments. X.M. Meng and
555 Y.G. Wu contributed to the experimental design and manuscript preparation. Y.T. Cai, M.F. Wu,
556 J.N. Wang, and Y.H. Dong performed the animal experiments. M.M. Liu, T.T. Ma, J.G. Wen, and
557 J. Li contributed new reagents or analytical tools**.**

558

559 **Funding**

560 This work was supported by the National Natural Science Foundation of China [grant number
561 81570623 and 81970584]; the Science and Technological Fund of Anhui Province for Outstanding
562 Youth of China [grant number 1608085J07]; and the Research Foundation Project of the Anhui
563 Institute of Translational Medicine [grant number 2017zhyx01].

564

565 **Declarations of interest**

566 The authors declare no conflicts of interest.

567

568 **Acknowledgements**

569 The authors thank the Center for Scientific Research of Anhui Medical University for valuable
570 help in our experiment. We would like to thank Editage for English language editing.

571

572 **References**

1. Pan T, Jia P, Chen N, Fang Y, Liang Y, Guo M, Ding X. Delayed Remote Ischemic Preconditioning ConfersRenoprotection against Septic Acute Kidney Injury via Exosomal miR-21. Theranostics. 2019;9(2):405-423.
2. Andrade-Silva M, Cenedeze MA, Perandini LA, Felizardo RJF, Watanabe IKM, Agudelo JSH, Castoldi A, Goncalves GM, Origassa CST, Semedo P, Hiyane MI, Foresto-Neto O, Malheiros D, Reis MA, Fujihara CK, Zatz R, Pacheco-Silva A, Camara NOS, de Almeida DC. TLR2 and TLR4 play opposite role in autophagy associated with cisplatin-induced acute kidney injury. Clin Sci (Lond). 2018;132(16):1725-1739.
3. Wang JN, Yang Q, Yang C, Cai YT, Xing T, Gao L, Wang F, Chen X, Liu XQ, He XY, Wei B, Jiang L, Li C, Jin J, Wen JG, Ma TT, Chen HY, Li J, Meng XM. Smad3 promotes AKI sensitivity in diabetic mice via interaction with p53 and induction of NOX4-dependent ROS production. Redox Biol. 2020;32:101479.
4. Gao L, Zhong X, Jin J, Li J, Meng XM. Potential targeted therapy and diagnosis based on novel insight into growth factors, receptors, and downstream effectors in acute kidney injury and acute kidney injury-chronic kidney disease progression. Signal Transduct Target Ther. 2020;5:9.
5. Shu S, Wang Y, Zheng M, Liu Z, Cai J, Tang C, Dong Z. Hypoxia and Hypoxia-Inducible Factors in Kidney Injury and Repair. Cells. 2019;8(3).
6. Hsu RK, McCulloch CE, Dudley RA, Lo LJ, Hsu CY. Temporal changes in incidence of dialysis-requiring AKI. J Am Soc Nephrol. 2013;24(1):37-42.
7. Li F, Liu Z, Tang C, Cai J, Dong Z. FGF21 is induced in cisplatin nephrotoxicity to protect against kidney tubular cell injury. FASEB J. 2018;32(6):3423-3433.
8. Sharfuddin AA, Molitoris BA. Pathophysiology of ischemic acute kidney injury. Nat Rev Nephrol. 2011;7(4):189-200.
9. Xu Y, Ma H, Shao J, Wu J, Zhou L, Zhang Z, Wang Y, Huang Z, Ren J, Liu S, Chen X, Han J. A Role for Tubular Necroptosis in Cisplatin-Induced AKI. J Am Soc Nephrol. 2015;26(11):2647-2658.
10. Gao L, Wu WF, Dong L, Ren GL, Li HD, Yang Q, Li XF, Xu T, Li Z, Wu BM, Ma TT, Huang C, Huang Y, Zhang L, Lv X, Li J, Meng XM. Protocatechuic Aldehyde Attenuates Cisplatin-Induced Acute Kidney Injury by Suppressing Nox-Mediated Oxidative Stress and Renal Inflammation. Front Pharmacol. 2016;7:479.
11. Meng XM, Li HD, Wu WF, Ming-Kuen Tang P, Ren GL, Gao L, Li XF, Yang Y, Xu T, Ma TT, Li Z, Huang C, Zhang L, Lv XW, Li J. Wogonin protects against cisplatin-induced acute kidney injury by targeting RIPK1-mediated necroptosis. Lab Invest. 2018;98(1):79-94.
12. Wu WF, Wang JN, Li Z, Wei B, Jin J, Gao L, Li HD, Li J, Chen HY, Meng XM. 7-Hydroxycoumarin protects against cisplatin-induced acute kidney injury by inhibiting necroptosis and promoting Sox9-mediated tubular epithelial cell proliferation. Phytomedicine. 2020;69:153202.
13. Ji L, Wu M, Li Z. Rutacecarpine Inhibits Angiogenesis by Targeting the VEGFR2 and VEGFR2-Mediated Akt/mTOR/p70s6k Signaling Pathway. Molecules. 2018;23(8).
14. Ueng YF, Tsai TH, Don MJ, Chen RM, Chen TL. Alteration of the pharmacokinetics of theophylline by rutaecarpine, an alkaloid of the medicinal herb Evodia rutaecarpa, in rats. J Pharm Pharmacol. 2005;57(2):227-232.

15. Ueng YF, Wang JJ, Lin LC, Park SS, Chen CF. Induction of cytochrome P450-dependent monooxygenase in mouse liver and kidney by rutaecarpine, an alkaloid of the herbal drug Evodia rutaecarpa. Life Sci. 2001;70(2):207-217.
16. Xu Y, Chen XP, Zhang F, Hou HH, Zhang JY, Lin SX, Sun AS. Rutaecarpine Inhibits Intimal Hyperplasia in A Balloon-Injured Rat Artery Model. Chin J Integr Med. 2018;24(6):429-435.
17. Wang C, Hao Z, Zhou J, Zhang L, Sun Y, Liang C. Rutaecarpine alleviates renal ischemia reperfusion injury in rats by suppressing the JNK/p38 MAPK signaling pathway and interfering with the oxidative stress response. Mol Med Rep. 2017;16(1):922-928.
18. Deng PY, Ye F, Cai WJ, Tan GS, Hu CP, Deng HW, Li YJ. Stimulation of calcitonin gene-related peptide synthesis and release: mechanisms for a novel antihypertensive drug, rutaecarpine. J Hypertens. 2004;22(9):1819-1829.
19. Wu M, Ma J, Ji L, Wang M, Han J, Li Z. Design, synthesis, and biological evaluation of rutacecarpine derivatives as multitarget-directed ligands for the treatment of Alzheimer's disease. Eur J Med Chem. 2019;177:198-211.
20. Deng J, Qin J, Cai Y, Zhong X, Zhang X, Yu S. Rutaecarpine Suppresses Proliferation and Promotes Apoptosis of Human Pulmonary Artery Smooth Muscle Cells in Hypoxia Possibly Through HIF-1alpha-Dependent Pathways. J Cardiovasc Pharmacol. 2018;71(5):293-302.
21. Dhuriya YK, Sharma D. Necroptosis: a regulated inflammatory mode of cell death. Journal of Neuroinflammation. 2018;15(1).
22. Meng XM, Ren GL, Gao L, Yang Q, Li HD, Wu WF, Huang C, Zhang L, Lv XW, Li J. NADPH oxidase 4 promotes cisplatin-induced acute kidney injury via ROS-mediated programmed cell death and inflammation. Lab Invest. 2018;98(1):63-78.
23. Yang Q, Ren GL, Wei B, Jin J, Huang XR, Shao W, Li J, Meng XM, Lan HY. Conditional knockout of TGF-betaRII /Smad2 signals protects against acute renal injury by alleviating cell necroptosis, apoptosis and inflammation. Theranostics. 2019;9(26):8277-8293.
24. Yang Q, Chen HY, Wang JN, Han HQ, Jiang L, Wu WF, Wei B, Gao L, Ma QY, Liu XQ, Chen Q, Wen JG, Jin J, Huang Y, Ni WJ, Ma TT, Li J, Meng XM. Alcohol promotes renal fibrosis by activating Nox2/4-mediated DNA methylation of Smad7. Clin Sci (Lond). 2020;134(2):103-122.
25. Lee DW, Kang Y, Kang MJ, Noh K, Kim JH, Nepal MR, Shakya R, Lee YJ, Jahng Y, Lee S, Kim JA, Jeong TC. Phase I and phase II metabolite identification of rutaecarpine in freshly isolated hepatocytes from male Sprague-Dawley rats. Arch Pharm Res. 2017;40(8):972-979.
26. Qin XP, Zeng SY, Tian HH, Deng SX, Ren JF, Zheng YB, Li D, Li YJ, Liao DF, Chen SY. Involvement of prolylcarboxypeptidase in the effect of rutaecarpine on the regression of mesenteric artery hypertrophy in renovascular hypertensive rats. Clin Exp Pharmacol Physiol. 2009;36(3):319-324.
27. Jiang J, Hu C. Evodiamine: a novel anti-cancer alkaloid from Evodia rutaecarpa. Molecules. 2009;14(5):1852-1859.
28. Yang L, Liu X, Wu D, Zhang M, Ran G, Bi Y, Huang H. Growth inhibition and induction of apoptosis in SGC7901 human gastric cancer cells by evodiamine. Mol Med Rep.

2014;9(4):1147-1152.

29. Zhong Z-F, Tan W, Wang S-P, Qiang W-A, Wang Y-T. Anti-proliferative activity and cell cycle arrest induced by evodiamine on paclitaxel-sensitive and -resistant human ovarian cancer cells. Scientific Reports. 2015;5(1).

30. Rabb H, Griffin MD, McKay DB, Swaminathan S, Pickkers P, Rosner MH, Kellum JA, Ronco C, Acute Dialysis Quality Initiative Consensus XWG. Inflammation in AKI: Current Understanding, Key Questions, and Knowledge Gaps. J Am Soc Nephrol. 2016;27(2):371-379.

31. Yang Q, Wu FR, Wang JN, Gao L, Jiang L, Li HD, Ma Q, Liu XQ, Wei B, Zhou L, Wen J, Ma TT, Li J, Meng XM. Nox4 in renal diseases: An update. Free Radic Biol Med. 2018;124:466-472.

32. Sureshbabu A, Ryter SW, Choi ME. Oxidative stress and autophagy: crucial modulators of kidney injury. Redox Biol. 2015;4:208-214.

33. Dennis JM, Witting PK. Protective Role for Antioxidants in Acute Kidney Disease. Nutrients. 2017;9(7).

34. Gao L, Liu MM, Zang HM, Ma QY, Yang Q, Jiang L, Ren GL, Li HD, Wu WF, Wang JN, Wei B, Liu XQ, Jiang C, Huang C, Li J, Meng XM. Restoration of E-cadherin by PPBICA protects against cisplatin-induced acute kidney injury by attenuating inflammation and programmed cell death. Lab Invest. 2018;98(7):911-923.

35. Gassanov N, Nia AM, Caglayan E, Er F. Remote ischemic preconditioning and renoprotection: from myth to a novel therapeutic option? J Am Soc Nephrol. 2014;25(2):216-224.

36. Paravicini TM, Touyz RM. NADPH oxidases, reactive oxygen species, and hypertension: clinical implications and therapeutic possibilities. Diabetes Care. 2008;31 Suppl 2:S170-180.

37. Kaysen GA, Eiserich JP. The role of oxidative stress-altered lipoprotein structure and function and microinflammation on cardiovascular risk in patients with minor renal dysfunction. J Am Soc Nephrol. 2004;15(3):538-548.

38. Alhasson F, Seth RK, Sarkar S, Kimono DA, Albadrani MS, Dattaroy D, Chandrashekaran V, Scott GI, Raychoudhury S, Nagarkatti M, Nagarkatti P, Diehl AM, Chatterjee S. High circulatory leptin mediated NOX-2-peroxynitrite-miR21 axis activate mesangial cells and promotes renal inflammatory pathology in nonalcoholic fatty liver disease. Redox Biol. 2018;17:1-15.

39. Xiao X, Du C, Yan Z, Shi Y, Duan H, Ren Y. Inhibition of Necroptosis Attenuates Kidney Inflammation and Interstitial Fibrosis Induced By Unilateral Ureteral Obstruction. Am J Nephrol. 2017;46(2):131-138.

40. Muller T, Dewitz C, Schmitz J, Schroder AS, Brasen JH, Stockwell BR, Murphy JM, Kunzendorf U, Krautwald S. Necroptosis and ferroptosis are alternative cell death pathways that operate in acute kidney failure. Cell Mol Life Sci. 2017;74(19):3631-3645.

41. Jiang L, Liu XQ, Ma Q, Yang Q, Gao L, Li HD, Wang JN, Wei B, Wen J, Li J, Wu YG, Meng XM. hsa-miR-500a-3P alleviates kidney injury by targeting MLKL-mediated necroptosis in renal epithelial cells. FASEB J. 2019;33(3):3523-3535.

42. Dhuriya YK, Sharma D. Necroptosis: a regulated inflammatory mode of cell death. J Neuroinflammation. 2018;15(1):199.

43. Ishii T, Okai T, Iwatani-Yoshihara M, Mochizuki M, Unno S, Kuno M, Yoshikawa M, Shibata S, Nakakariya M, Yogo T, Kawamoto T. CETSA quantitatively verifies in vivo target engagement of novel RIPK1 inhibitors in various biospecimens. Sci Rep. 2017;7(1):13000.
44. von Massenhausen A, Tonnus W, Linkermann A. Cell Death Pathways Drive Necroinflammation during Acute Kidney Injury. Nephron. 2018;140(2):144-147.
45. Qian Y, Guo X, Che L, Guan X, Wu B, Lu R, Zhu M, Pang H, Yan Y, Ni Z, Gu L. Klotho Reduces Necroptosis by Targeting Oxidative Stress Involved in Renal Ischemic-Reperfusion Injury. Cell Physiol Biochem. 2018;45(6):2268-2282.
46. Jackson EK, Menshikova EV, Mi Z, Verrier JD, Bansal R, Janesko-Feldman K, Jackson TC, Kochanek PM. Renal 2',3'-Cyclic Nucleotide 3'-Phosphodiesterase Is an Important Determinant of AKI Severity after Ischemia-Reperfusion. J Am Soc Nephrol. 2016;27(7):2069-2081.
47. Ju-Rong Y, Ke-Hong C, Kun H, Bi-Qiong F, Li-Rong L, Jian-Guo Z, Kai-Long L, Ya-Ni H. Transcription Factor Trps1 Promotes Tubular Cell Proliferation after Ischemia-Reperfusion Injury through cAMP-Specific 3',5'-Cyclic Phosphodiesterase 4D and AKT. J Am Soc Nephrol. 2017;28(2):532-544.
48. Lugnier C. Cyclic nucleotide phosphodiesterase (PDE) superfamily: a new target for the development of specific therapeutic agents. Pharmacol Ther. 2006;109(3):366-398.
49. Ghosh M, Garcia-Castillo D, Aguirre V, Golshani R, Atkins CM, Bramlett HM, Dietrich WD, Pearse DD. Proinflammatory cytokine regulation of cyclic AMP-phosphodiesterase 4 signaling in microglia in vitro and following CNS injury. Glia. 2012;60(12):1839-1859.
50. Pearse DD, Pereira FC, Marcillo AE, Bates ML, Berrocal YA, Filbin MT, Bunge MB. cAMP and Schwann cells promote axonal growth and functional recovery after spinal cord injury. Nat Med. 2004;10(6):610-616.
51. Li H, Fan C, Feng C, Wu Y, Lu H, He P, Yang X, Zhu F, Qi Q, Gao Y, Zuo J, Tang W. Inhibition of phosphodiesterase-4 attenuates murine ulcerative colitis through interference with mucosal immunity. Br J Pharmacol. 2019;176(13):2209-2226.
52. Holthoff JH, Wang Z, Patil NK, Gokden N, Mayeux PR. Rolipram improves renal perfusion and function during sepsis in the mouse. J Pharmacol Exp Ther. 2013;347(2):357-364.
53. Jin SL, Lan L, Zoudilova M, Conti M. Specific role of phosphodiesterase 4B in lipopolysaccharide-induced signaling in mouse macrophages. J Immunol. 2005;175(3):1523-1531.
54. Pearse DD, Hughes ZA. PDE4B as a microglia target to reduce neuroinflammation. Glia. 2016;64(10):1698-1709.
55. Myers SA, Gobejishvili L, Saraswat Ohri S, Garrett Wilson C, Andres KR, Riegler AS, Donde H, Joshi-Barve S, Barve S, Whittemore SR. Following spinal cord injury, PDE4B drives an acute, local inflammatory response and a chronic, systemic response exacerbated by gut dysbiosis and endotoxemia. Neurobiol Dis. 2019;124:353-363.
56. Cheng J, Grande JP. Cyclic nucleotide phosphodiesterase (PDE) inhibitors: novel therapeutic agents for progressive renal disease. Exp Biol Med (Maywood). 2007;232(1):38-51.
57. Dousa TP. Cyclic-3',5'-nucleotide phosphodiesterase isozymes in cell biology and

pathophysiology of the kidney. Kidney Int. 1999;55(1):29-62.

58. Ding H, Bai F, Cao H, Xu J, Fang L, Wu J, Yuan Q, Zhou Y, Sun Q, He W, Dai C, Zen K, Jiang L, Yang J. PDE/cAMP/Epac/C/EBP-β Signaling Cascade Regulates Mitochondria Biogenesis of Tubular Epithelial Cells in Renal Fibrosis. Antioxidants & Redox Signaling. 2018;29(7):637-652.

59. Rodriguez WE, Wahlang B, Wang Y, Zhang J, Vadhanam MV, Joshi-Barve S, Bauer P, Cannon R, Ahmadi AR, Sun Z, Cameron A, Barve S, Maldonado C, McClain C, Gobejishvili L. Phosphodiesterase 4 Inhibition as a Therapeutic Target for Alcoholic Liver Disease: From Bedside to Bench. Hepatology. 2019.

60. Wang JN, Liu MM, Wang F, Wei B, Yang Q, Cai YT, Chen X, Liu XQ, Jiang L, Li C, Hu XW, Yu JT, Ma TT, Jin J, Wu YG, Li J, Meng XM. RIPK1 inhibitor Cpd-71 attenuates renal dysfunction in cisplatin-treated mice via attenuating necroptosis, inflammation and oxidative stress. Clin Sci (Lond). 2019;133(14):1609-1627.

Figure Legends

Figure 1. The formula of rutaecarpine and 3-aromatic sulphonamide-substituted rutaecarpine derivatives (A) The molecular formula and structure of rutaecarpine and 3-aromatic sulphonamide-substituted rutaecarpine derivatives. (B)1H NMR, 13C NMR and HRMS spectra for Cpd-6c.

Figure 2. Effect of rutaecarpine and its derivatives on cisplatin-treated HK2 cell viability. (A) Effect of varying concentrations of rutaecarpine and its derivatives on HK2 cell viability and cisplatin-treated HK2 cell viability (MTT assay). *p < 0.05, **p < 0.01, ***p < 0.001 compared to the control. #*p* < 0.05, ##*p* < 0.01, ###*p* < 0.001 compared to the cisplatin-treated group. Abbreviation: Cis, cisplatin

Figure 3. Effect of Cpd-6c and Cpd-6b on cell injury. (A) Western blot analysis of KIM-1 in HK2 cells. (B) Real-time PCR analyses of KIM-1 mRNA levels. (C) IF of KIM-1 in HK2 cells. (D) PI/Annexin-V flow cytometry. (E) Quantitative western blot data analysis. Data represent the mean + SEM for 3–4 independent experiments. *p < 0.05, **p < 0.01, ***p < 0.001 compared to the control. #*p* < 0.05, ##*p* < 0.01, ###*p* < 0.001 compared to the cisplatin-treated group. Scale bar = 100μm. Abbreviation: Cis, cisplatin

Figure 4. Cpd-6c inhibits cisplatin-induced inflammation and oxidative stress in HK2 cells.

(A) Quantitative data analysis of western blot of P-P65. (B) Real-time PCR analyses of renal

TNF-α, IL-1β, and IL-8 mRNA levels. (C) Quantitative western blot data analysis of cisplatin-treated HK2 cells. (D) DCF assay for reactive oxygen species. (E) DHE staining for intracellular ROS levels. Data represent the mean ± SEM for 3–4 independent experiments. *p < 0.05, **p < 0.01, ***p < 0.001 compared to the control. #*p* < 0.05, ##*p* < 0.01, ###*p* < 0.001 compared to cisplatin-treated group. Scale bar = 100μm. Abbreviation: Cis, cisplatin

Figure 5. Prediction of Cpd-6c molecular targets. (A) Profiling of the predicted protein targets of Cpd-6c via DS 2017. The y-axis represents the compound Cpd-6c, and the x-axis indicates the predicted pharmacophore models (pharmacological targets) of Cpd-6c. The colour from blue to red represents a high fit value and a better fit. (B) ELISA experiments using serum from healthy volunteers and patients with AKI to detect PDE4B release. (C) CETSA analysis of the stabilization of PDE4B with or without Cpd-6c treatment. (D) Molecular docking. (E) IF of PDE4B in HK2 cells. (F) IF of cAMP in HK2 cells. Data represent the mean ± SEM for 3–4 independent experiments. *p < 0.05, **p < 0.01, ***p < 0.001 compared to the control. #*p* < 0.05, ##*p* < 0.01, ###*p* < 0.001 compared to cisplatin-treated group. Scale bars = 100μm. Abbreviation: Cis, cisplatin

Figure 6. Cpd-6c fails to further reduce the cisplatin-induced cell injury in PDE4B instead of PDE10A and PDE4D-silenced HK2 cells. (A) Real-time PCR (B) Quantitative western blot analysis. (C) Quantitative data analysis of western blot of PDE4B in cisplatin-treated HK2 cells. **(**D) Quantitative data analysis of western blot of KIM-1 in PDE4B-silenced HK2 cells. (E) Real-time PCR. **(**E) Quantitative data analysis of western blot of KIM-1 in PDE4D-silenced HK2 cells. **(**F) Quantitative data analysis of western blot of KIM-1 in PDE10A-silenced HK2 cells. Data represent the mean ± SEM for 3–4 independent experiments. *p < 0.05, **p < 0.01, ***p < 0.001 compared to the control. #p < 0.05, ##p < 0.01, ###p < 0.001 compared with the PDE4B EV group. $p < 0.05, $$p < 0.01, $$$p < 0.001 compared to the cisplatin-treated group. Abbreviation: Cis, cisplatin. EV, empty vector; KD, knockdown

Figure 7. Cpd-6c fails to reduce the cisplatin-induced cell death, inflammatory response and oxidative stress in PDE4B-silenced HK2 cells further. (A) Quantitative data analysis of western blot of cleaved caspase-3. (B) Quantitative data analysis of western blot of P-P65. (C) Real-time PCR of TNF-α, IL-1β, IL-8 in mRNA levels. (D) Quantitative data analysis of western blot of NADPH oxidase proteins. Data represent the mean ± SEM for 3–4 independent experiments. *p < 0.05, **p < 0.01, ***p < 0.001 compared to the control. #p < 0.05, ##p < 0.01, ###p < 0.001 compared to PDE4B EV group. $p < 0.05, $$p < 0.01, $$$p < 0.001 compared to cisplatin-treated group. Abbreviation: Cis, cisplatin; EV, empty vector; KD, knockdown

Figure 8. Targeting PDE4B with Cpd-6c exhibits a superior protective effect in cisplatin-induced cell injury compared to that observed upon using the classical PDE4 inhibitor rolipram.

(A) Effect of varying concentrations of rolipram on HK2 cell viability (MTT assay). (B) Rolipram restores the viability in cisplatin-treated HK2 cells (MTT assay). (C) and (D) Cpd-6c exerts a stronger suppressive effect on KIM-1 than rolipram. (E) Cpd-6c displays a greater inhibitory effect on cisplatin-induced apoptosis compared to rolipram. (F) and (G) Cpd-6c exhibits a stronger inhibitory effect on inflammation than rolipram. (H) Cpd-6c displays a greater inhibitory effect on cisplatin-induced oxidative stress compared to rolipram. Data represent the mean ± SEM for 3–4 independent experiments. *p < 0.05, **p < 0.01, ***p < 0.001 compared to the control. #p < 0.05, ##p < 0.01, ###p < 0.001 compared to the cisplatin-treated group. Abbreviation: Cis, cisplatin

Figure 9. Cpd-6c prevents *in vivo* cisplatin-induced renal injury and a decline in renal function. (A) Serum creatinine. (B) BUN. (C) PAS staining and score. (D), (E), and (F) Western blot analysis, real-time PCR, and immunohistochemistry of KIM-1. Data represent the mean ± SEM for 3–4 independent experiments. *p < 0.05, **p < 0.01, ***p < 0.001 compared to the control. #*p* < 0.05, ##*p* < 0.01, ###*p* < 0.001 compared to cisplatin-treated group. Scale bar = 100μm. Abbreviation: Cis, cisplatin

Figure 10. Cpd-6c decreases PDE4B level and programmed cell death in cisplatin nephropathy.

(A)and(B)western blot analysis and immunohistochemistry of PDE4B. (C) Quantitative data analysis of western blot of RIPK1, RIPK3, p-MLKL, and cleaved caspase-3. Data represent the mean ± SEM for 6–8 mice. Data represent the mean ± SEM for 6–8 mice. *p < 0.05, **p < 0.01, ***p < 0.001 compared to control. #*p* < 0.05, ##*p* < 0.01, ###*p* < 0.001 compared to model. Scale bar = 100μm. Abbreviation: Cis, cisplatin

Figure 11. Cpd-6c attenuates *in vivo* cisplatin-induced renal inflammation and oxidative stress.

(A) Real-time PCR of inflammation indices. (B) Quantitative data analysis of western blot of P-P65. (C) Immunohistochemistry of TNF-a. (D) Quantitative data analysis of western blot of NOX1, NOX2, and NOX4. Data represent the mean ± SEM for 6–8 mice. Data represent the mean ± SEM for 6–8 mice. *p < 0.05, **p < 0.01, ***p < 0.001 compared to control. #*p* < 0.05, ##*p* < 0.01, ###*p* < 0.001 compared to model. Scale bar = 100μm. Abbreviation: Cis, cisplatin

Figure 12. Cpd-6c attenuated cisplatin-induced kidney injury in established AKI mouse

model. (A) Serum creatinine. (B) BUN. (C) PAS staining and score. (D) Western blot analysis of KIM-1. Data represent the mean ± SEM for 3–4 independent experiments. *p < 0.05, **p < 0.01, ***p < 0.001 compared to the control. #*p* < 0.05, ##*p* < 0.01, ###*p* < 0.001 compared to cisplatin-treated group. Scale bar = 100μm. Abbreviation: Cis, cisplatin

Table 1. Primer sequences used in real-time PCR

Genes	Forward primer (5'–3')	Forward primer (5'–3')
Human IL-8	AGGACAAGAGCCAGGAAGAA	ACTGCACCTTCACACAGAGC
Human TNF-α	CCCAGGGACCTCTCTCTAATCA	GCTACAGGCTTGTCACTCGG
Human KIM-1	CTGCAGGGAGCAATAAGGAG	TCCAAAGGCCATCTGAAGAC
Human β-actin	CGCCGCCAGCTCACCATG	CACGATGGAGGGGAAGACGG
Mouse IL-6	GAGGATACCACTCCCAACAGACC	AAGTGCATCATCGTTGTTCATACA
Mouse MCP-1	CTTCTGGGCCTGCTGTTCA	CCAGCCTACTCATTGGGATCA
Mouse KIM-1	CAGGGAAGCCGCAGAAAA	GAGACACGGAAGGCAACCAC
Mouse TNF-a	CATCTTCTCAAAATTCGAGTGACAA	TGGGAGTAGACAAGGTACAACCC
Mouse β-actin	CATTGCTGACAGGATGCAGAA	ATGGTGCTAGGAGCCAGAGC

Table 2. Top ten putative protein targets of Cpd-6c predicted using Discovery Studio 2017

Rank	PDB ID [a]	Putative Target	Fit Value [b]
1	1tbb	cAMP-specific 3',5'-cyclic phosphodiesterase 4D	0.9933
2	1xlx	cAMP-specific 3',5'-cyclic phosphodiesterase 4B	0.9868
3	2o8h	Phosphodiesterase-10A	0.9864
4	1xlz	cAMP-specific 3',5'-cyclic phosphodiesterase 4B	0.9846
5	7std	Scytalone dehydratase	0.9830
6	2gz7	Replicase polyprotein 1ab	0.9799
7	2jh6	Thrombin	0.9762
8	1t47	4-hydroxyphenylpyruvate dioxygenase	0.9727
9	3lbj	MDM4 protein	0.9660
10	3b3k	Peroxisome proliferator-activated receptor gamma	0.9644

Credit Author Statement

Xueqi Liu: Investigation, Acquisition of the data, Analysis and interpretation of the data,Writing, review and/or revision of the manuscript

Juan Jin: Investigation, Analysis and interpretation of the data

Zeng Li: Conceptualization, Formal analysis, Funding acquisition

Ling Jiang: Investigation, Acquisition of the data, Analysis and interpretation of the data

Yuhang Dong: Investigation, Analysis of the data

Yuting Cai: Validation

Mingfei Wu: Validation, Software

Jianan Wang: Investigation, Acquisition of the data

Taotao Ma: Investigation

Jiagen Wen: Investigation, Acquisition of the data

Jun Li: Investigation

Yonggui Wu: Conception and design, Supervision, Writing - review & editing

Xiaoming Meng: Conception and design, Funding acquisition, Supervision, Writing - original draft,Writing - review & editing

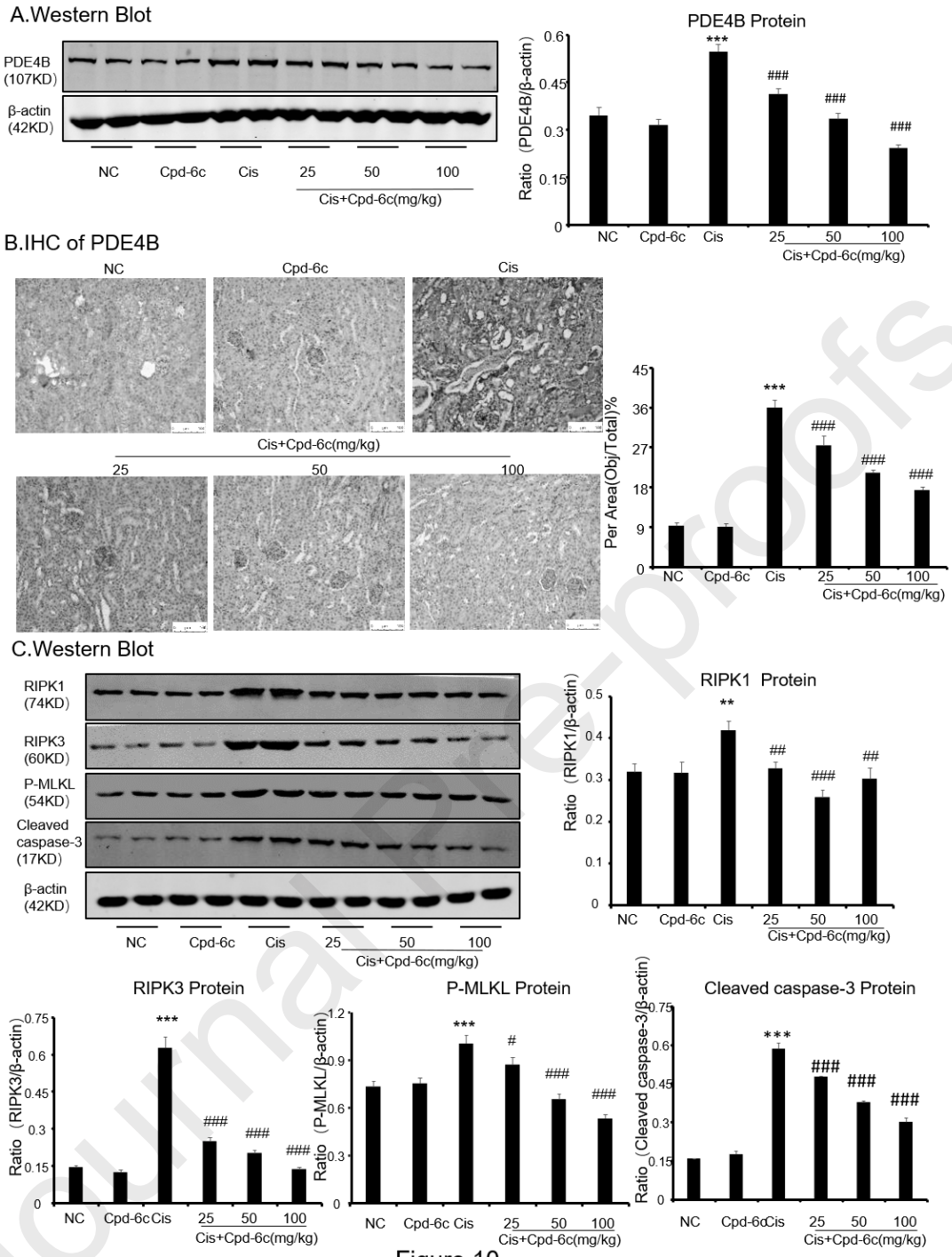

Figure 10

887

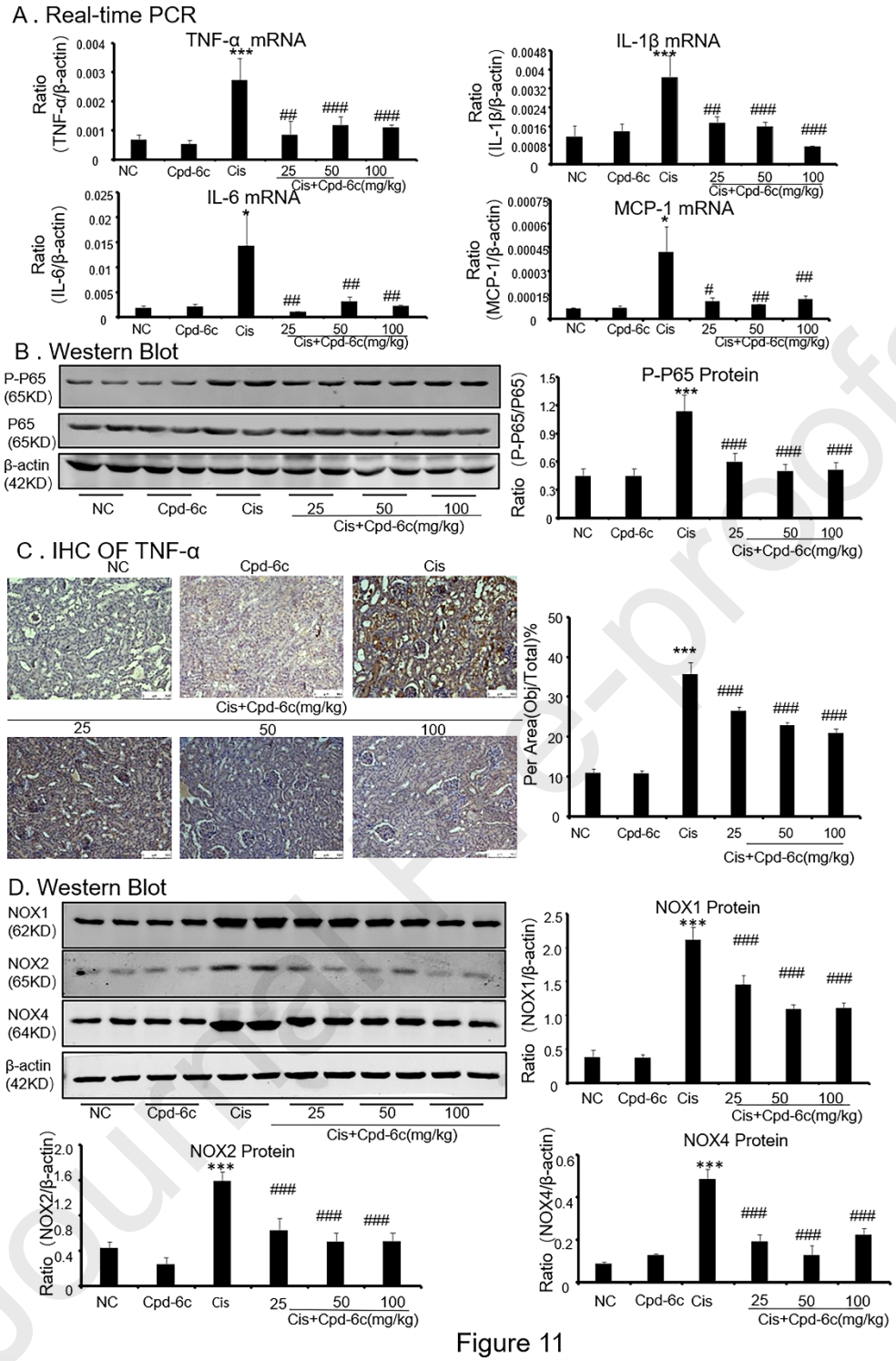
A . Real-time PCR
TNF-α mRNA
Ratio (TNF-α/β-actin)
IL-1β mRNA
Ratio (IL-1β/β-actin)
IL-6 mRNA
Ratio (IL-6/β-actin)
MCP-1 mRNA
Ratio (MCP-1/β-actin)
NC
Cpd-6c
Cis
25
50
100
Cis+Cpd-6c(mg/kg)
B . Western Blot
P-P65 (65KD)
P65 (65KD)
β-actin (42KD)
P-P65 Protein
Ratio (P-P65/P65)
C . IHC OF TNF-α
Per Area(Obj/Total)%
D. Western Blot
NOX1 (62KD)
NOX2 (65KD)
NOX4 (64KD)
β-actin (42KD)
NOX1 Protein
Ratio (NOX1/β-actin)
NOX2 Protein
Ratio (NOX2/β-actin)
NOX4 Protein
Ratio (NOX4/β-actin)

Figure 11

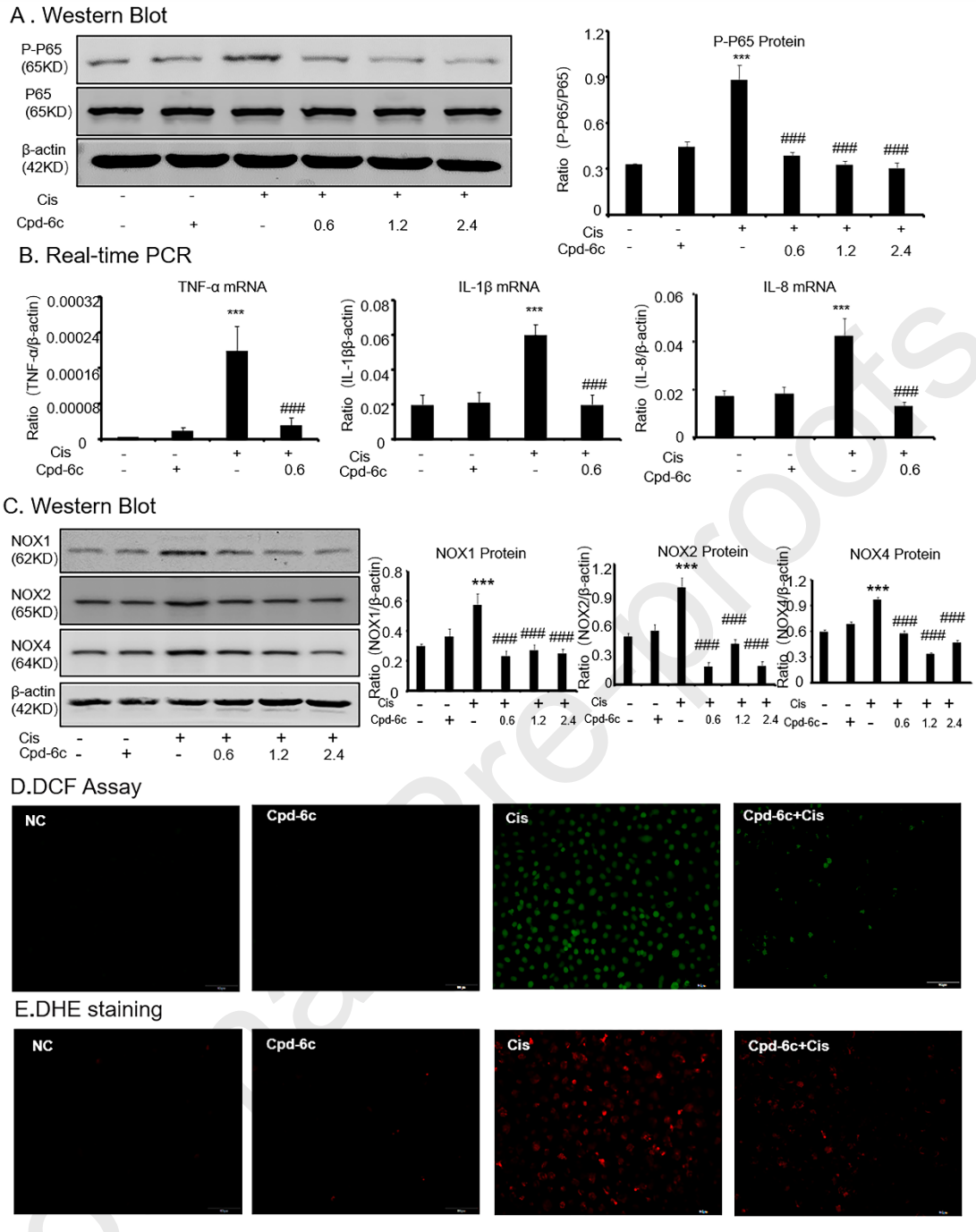
A . Western Blot
P-P65 (65KD)
P65 (65KD)
β-actin (42KD)
Cis
Cpd-6c
P-P65 Protein
Ratio (P-P65/P65)
B. Real-time PCR
TNF-α mRNA
IL-1β mRNA
IL-8 mRNA
C. Western Blot
NOX1 (62KD)
NOX2 (65KD)
NOX4 (64KD)
NOX1 Protein
NOX2 Protein
NOX4 Protein
D.DCF Assay
NC
Cpd-6c
Cis
Cpd-6c+Cis
E.DHE staining

Figure 4

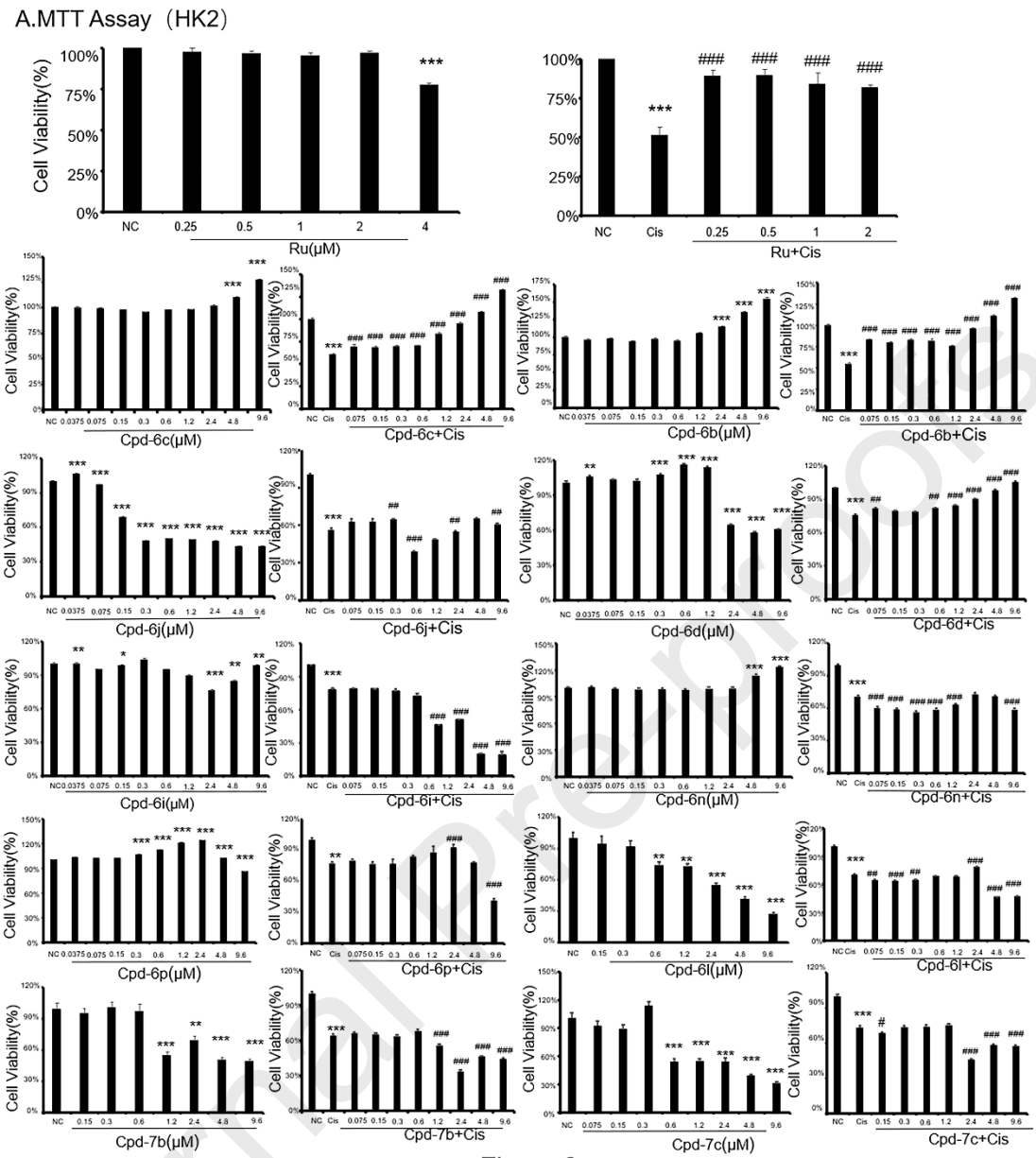

Figure 2

890

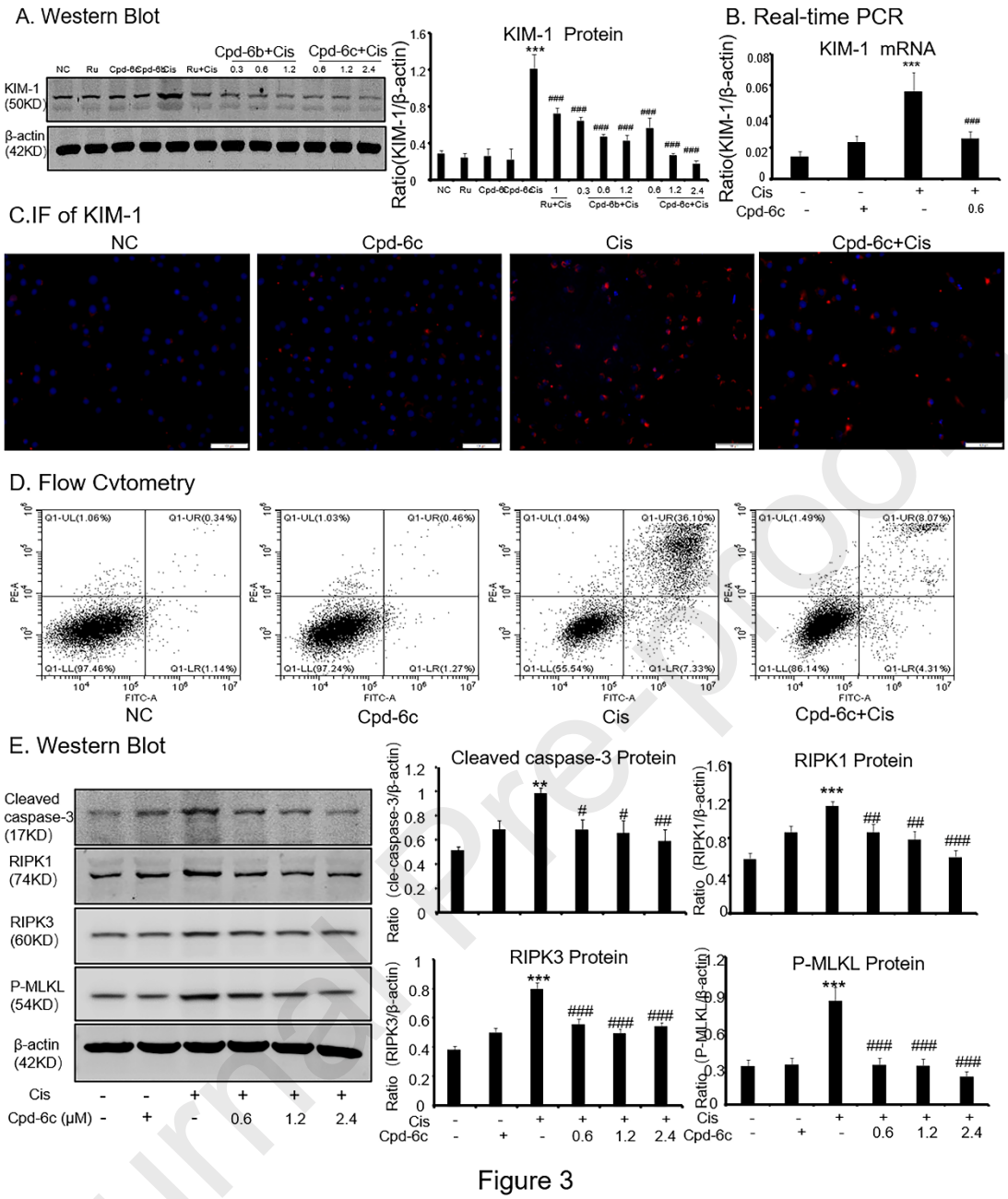

Figure 3

891

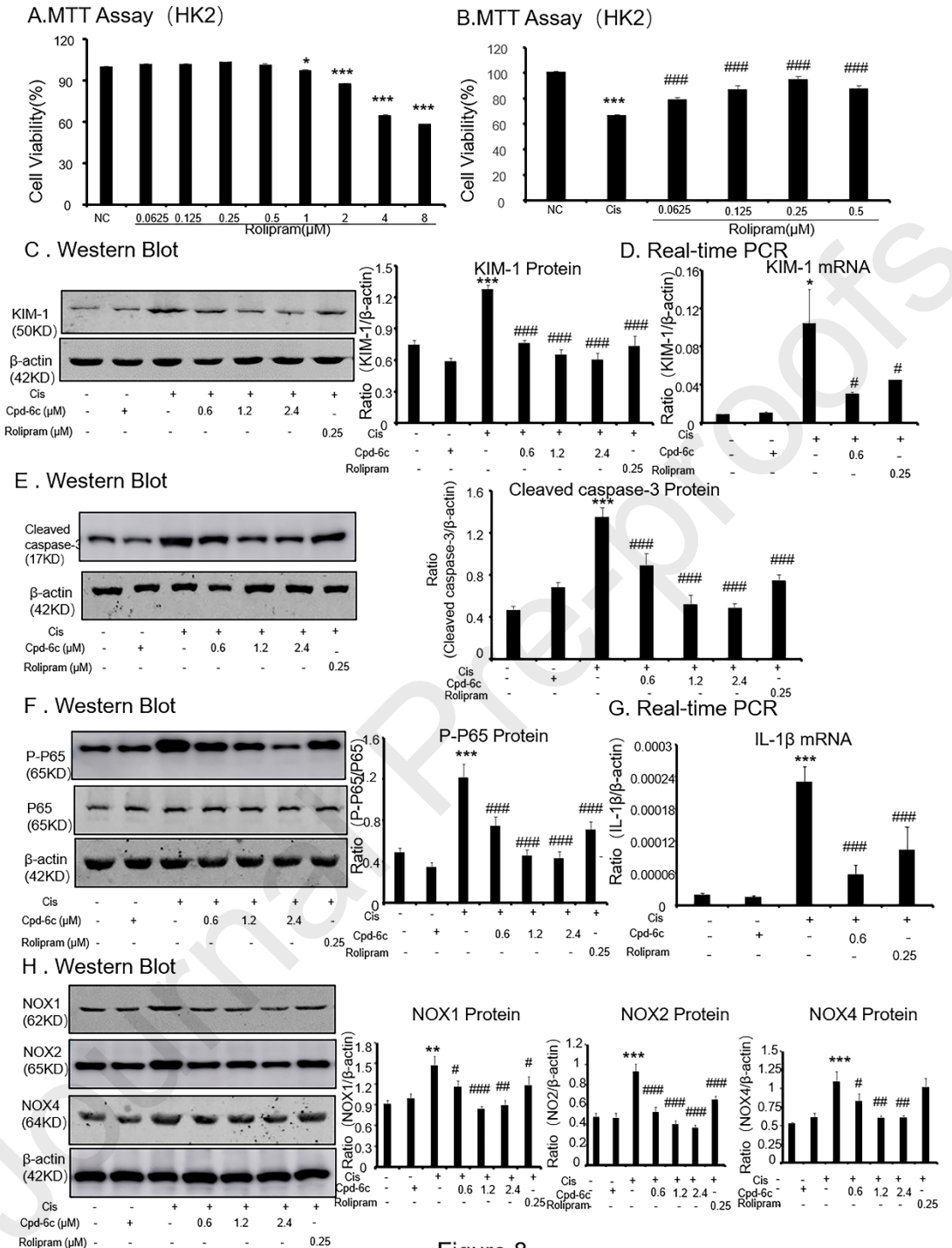
A.MTT Assay（HK2）
Cell Viability(%)
Rolipram(μM)
B.MTT Assay（HK2）
Cell Viability(%)
Rolipram(μM)
C . Western Blot
KIM-1 (50KD)
β-actin (42KD)
Cis
Cpd-6c (μM)
Rolipram (μM)
KIM-1 Protein
Ratio (KIM-1/β-actin)
D. Real-time PCR
KIM-1 mRNA
Ratio (KIM-1/β-actin)
E . Western Blot
Cleaved caspase-3 (17KD)
β-actin (42KD)
Cleaved caspase-3 Protein
Ratio (Cleaved caspase-3/β-actin)
F . Western Blot
P-P65 (65KD)
P65 (65KD)
β-actin (42KD)
P-P65 Protein
Ratio (P-P65/P65)
G. Real-time PCR
IL-1β mRNA
Ratio (IL-1β/β-actin)
H . Western Blot
NOX1 (62KD)
NOX2 (65KD)
NOX4 (64KD)
β-actin (42KD)
NOX1 Protein
NOX2 Protein
NOX4 Protein
Ratio (NOX1/β-actin)
Ratio (NO2/β-actin)
Ratio (NOX4/β-actin)

Figure 8

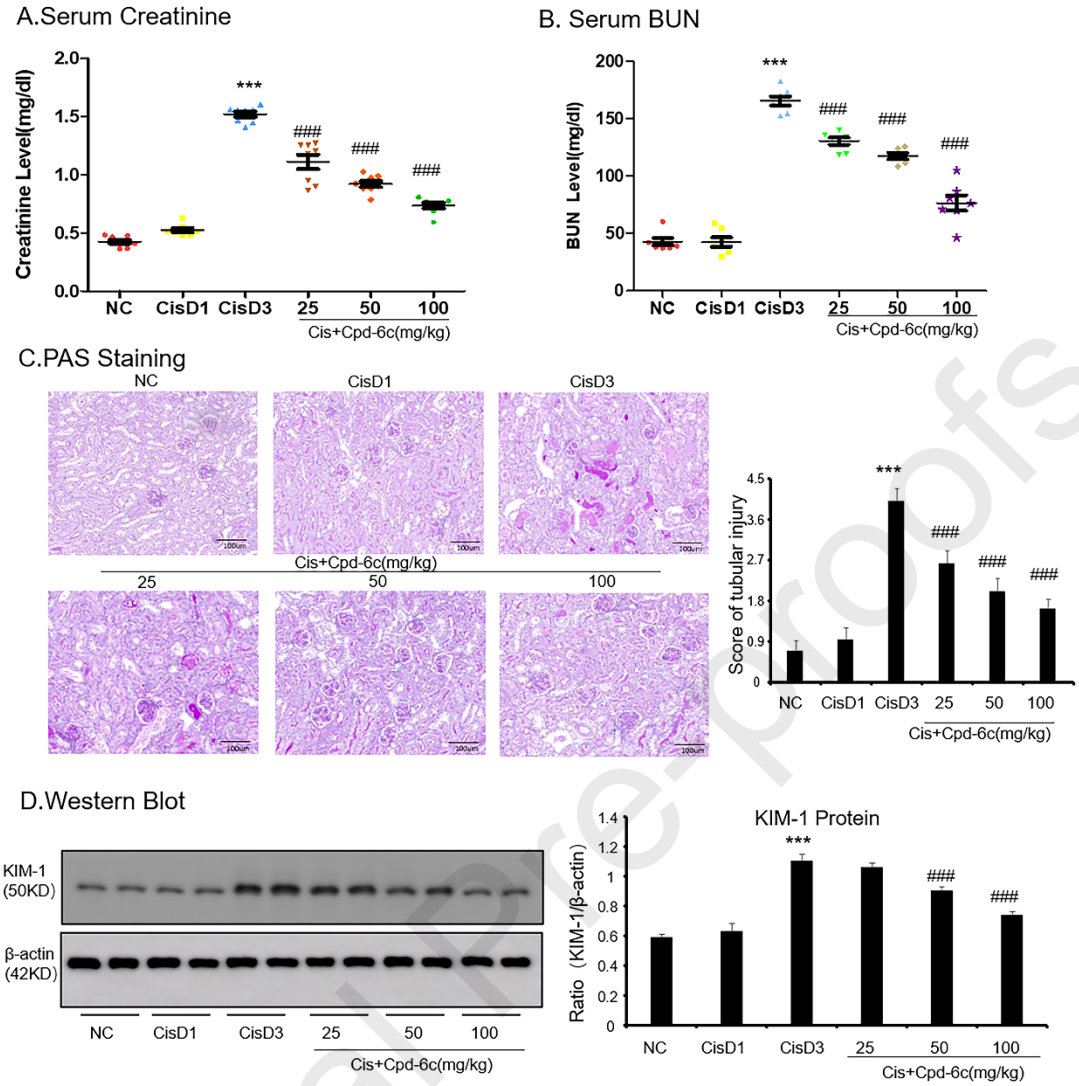

Figure 12

893

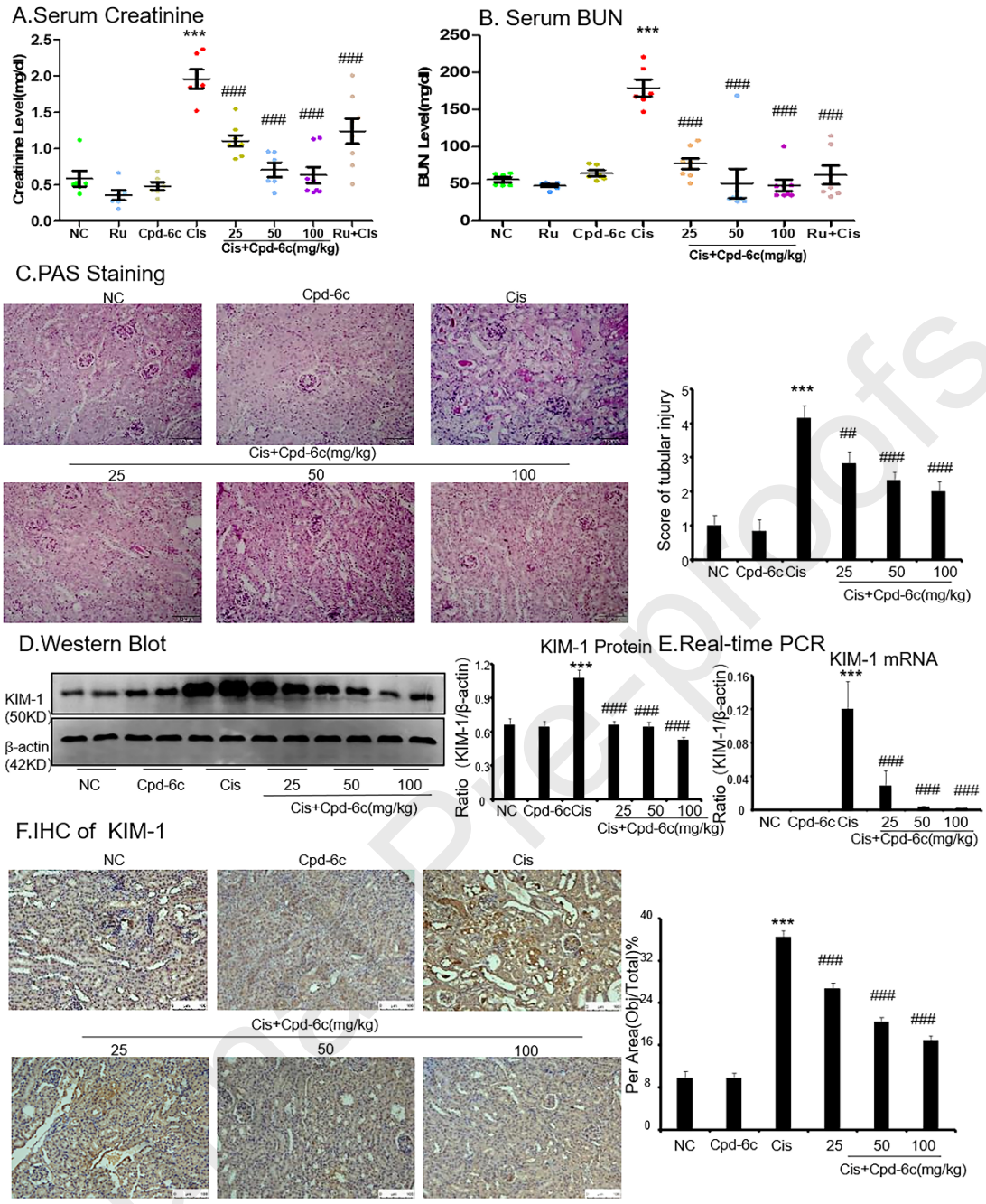
A.Serum Creatinine
Creatinine Level(mg/dl)
NC Ru Cpd-6c Cis 25 50 100 Ru+Cis
Cis+Cpd-6c(mg/kg)
B. Serum BUN
BUN Level(mg/dl)
C.PAS Staining
NC
Cpd-6c
Cis
Cis+Cpd-6c(mg/kg)
25
50
100
Score of tubular injury
D.Western Blot
KIM-1 (50KD)
β-actin (42KD)
KIM-1 Protein
Ratio (KIM-1/β-actin)
E.Real-time PCR
KIM-1 mRNA
F.IHC of KIM-1
Per Area(Obj/Total)%

Figure 9

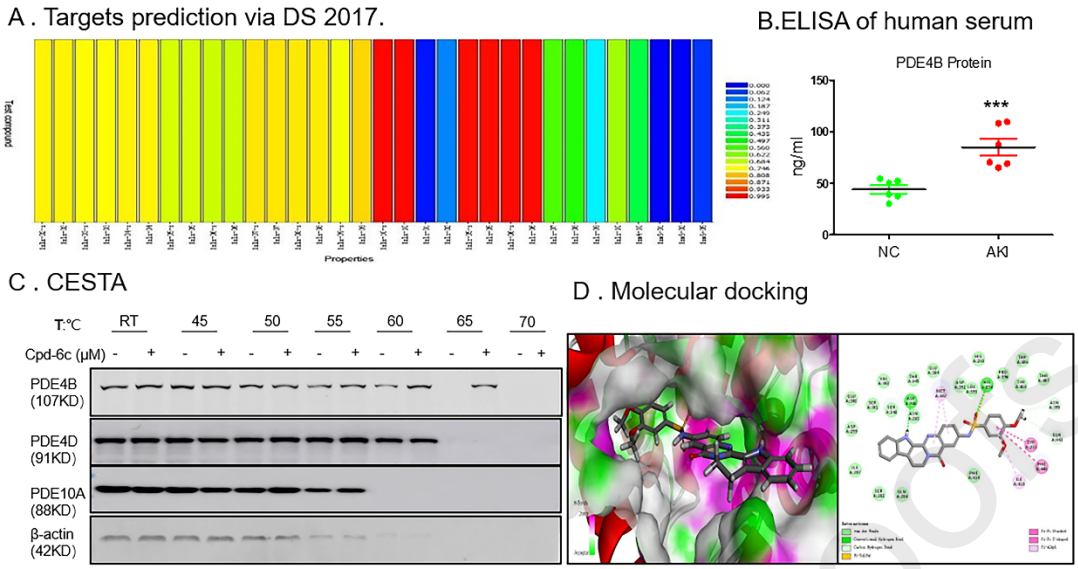

Figure 5

895

A. Molecular structure

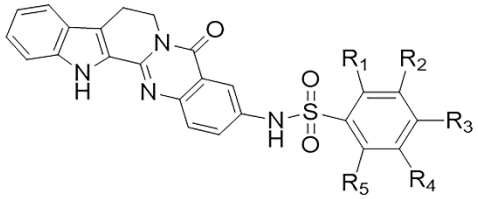

Rutaecarpine

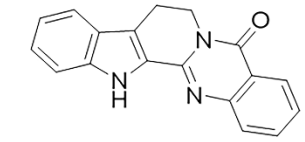

6j : R_1=R_2=R_4=R_5=H, R_3=$C(CH_3)_3$
6d : R_1=R_2=R_4=R_5=H, R_3=NO_2
6i : R_1=R_4=R_5=H, R_2=Cl, R_3=F
6c : R_1=R_4=R_5=H, R_2=R_3=OCH_3
6n : R_2=R_3=R_4=R_5=H, R_1=OCF_3
6p : R_1=R_2=R_4=R_5=H, R_3=$COCH_3$
6b : R_2=R_4=R_5=H, R_1=R_3=OCH_3
6l : R_1=R_2=R_4=R_5=H, R_3=OCF_3

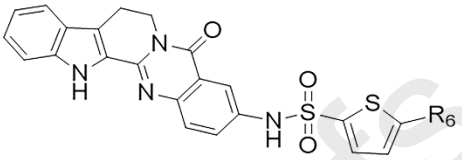

7b : R_6=Br
7c : R_6=Cl

B. Minimum characterization

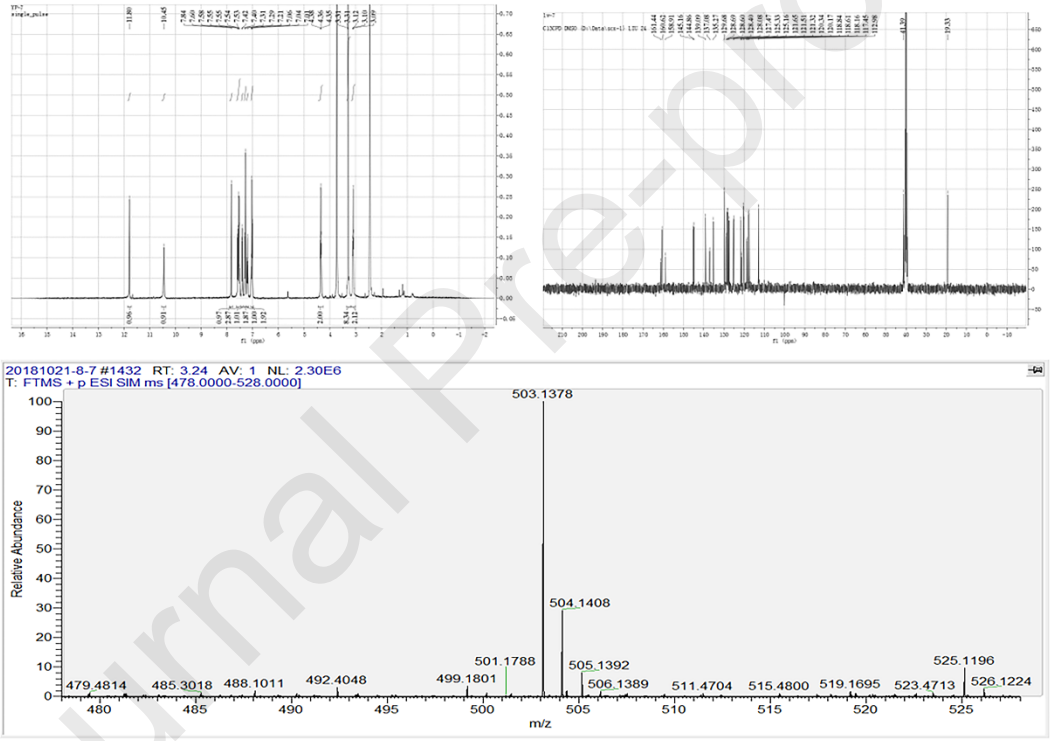

Figure 1

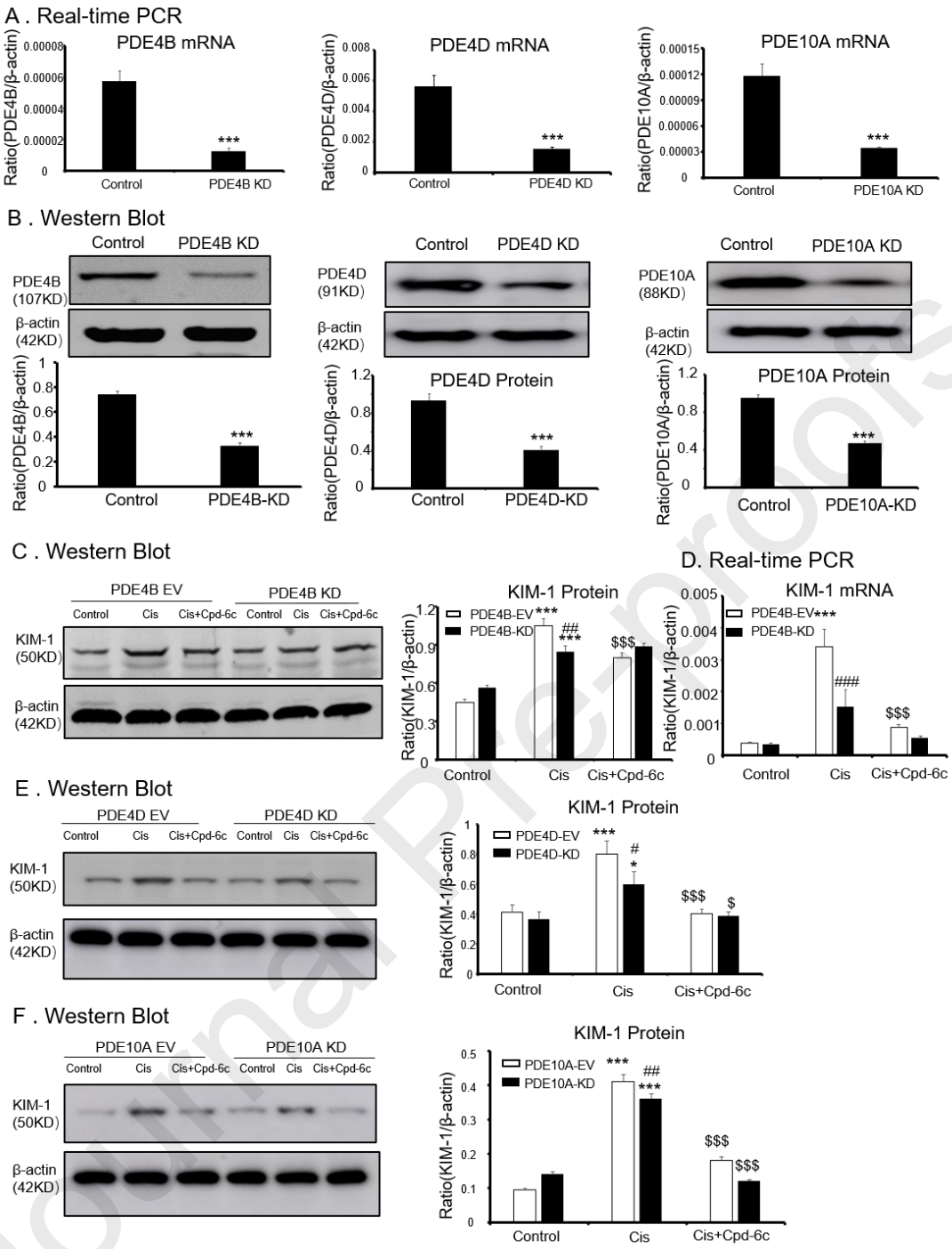
A . Real-time PCR
PDE4B mRNA
Ratio(PDE4B/β-actin)
Control
PDE4B KD
PDE4D mRNA
Ratio(PDE4D/β-actin)
PDE4D KD
PDE10A mRNA
Ratio(PDE10A/β-actin)
PDE10A KD
B . Western Blot
PDE4B (107KD)
β-actin (42KD)
PDE4B-KD
PDE4D (91KD)
PDE4D-KD
PDE10A (88KD)
PDE10A-KD
PDE4D Protein
PDE10A Protein
C . Western Blot
PDE4B EV
PDE4B KD
Cis
Cis+Cpd-6c
KIM-1 (50KD)
KIM-1 Protein
PDE4B-EV
PDE4B-KD
D. Real-time PCR
KIM-1 mRNA
E . Western Blot
PDE4D EV
PDE4D KD
PDE4D-EV
PDE4D-KD
F . Western Blot
PDE10A EV
PDE10A KD
PDE10A-EV
PDE10A-KD

Figure 6

898

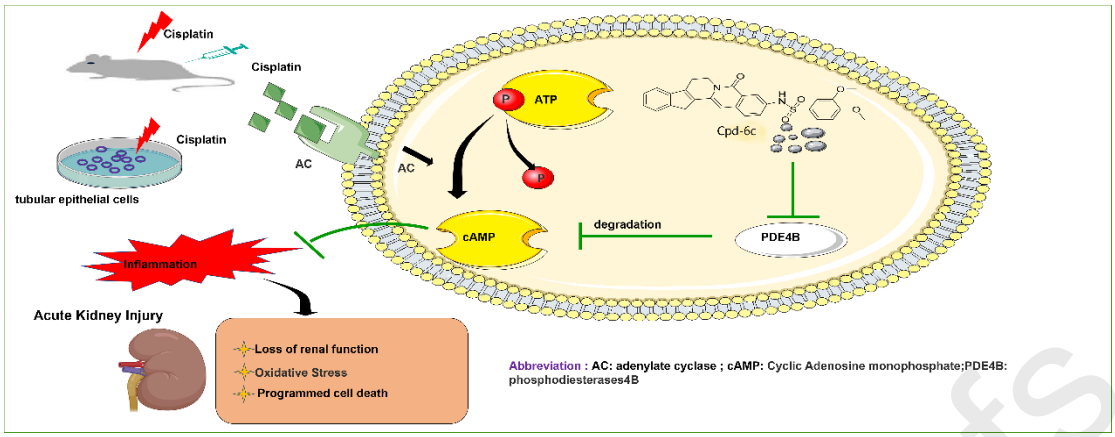

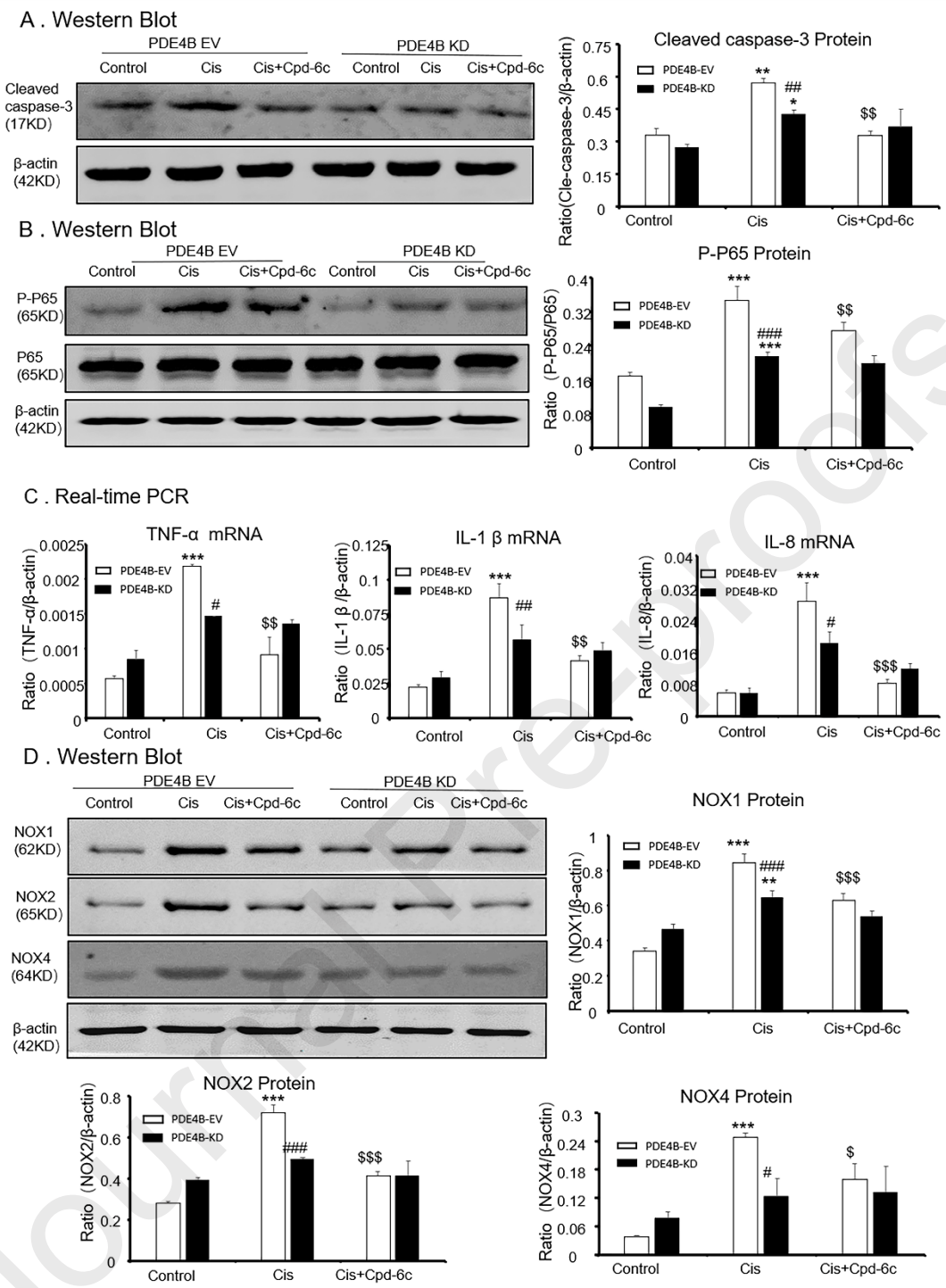

Figure 7